ACS Energy LETTERS

http://pubs.acs.org/journal/aelccp

REVIEW

Toward Maximizing Hole Selection with Self-Assembled Monolayers in Sn-Based Perovskite Solar Cells

Donghoon Song,* Seung Wook Shin, Hui-Ping Wu, Eric Wei-Guang Diau,* and Juan-Pablo Correa-Baena*

Cite This: *ACS Energy Lett.* 2025, 10, 1292−1312

Read Online

ACCESS | Metrics & More | Article Recommendations | Supporting Information

ABSTRACT: Even though hole-selective self-assembled monolayers (SAMs) are a key player for light management and carrier management in Pb- and Sn−Pb based perovskite solar cells (PSCs), they are markedly underdeveloped for Sn PSCs. Herein, we offer multifaceted approaches as a roadmap to tackle this challenge. We systematically reviewed recent publications on Sn PSCs utilizing hole-selective SAMs to identify underexplored approaches and suboptimal photovoltaic performance. We then examined state-of-the-art PSCs based on Pb and Sn−Pb perovskites to induce their success to arise from multifaceted approaches on the substrate, SAM, perovskite, and their interfaces. Additionally, we emphasized the unique underlying properties of Sn PSCs that warrant careful consideration. Finally, we proposed feasible approaches to improve the SAM-based Sn PSCs, in light of light management and carrier management, by leveraging the unique properties of Sn perovskites alongside the multifaceted approaches proven effective in other PSCs.

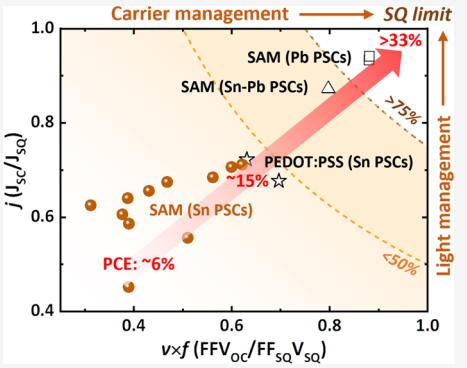

A self-assembled monolayer (SAM) is a thin and compact film (thickness: ca. 1−5 nm) composed of small molecules that are chemically and physically adsorbed onto a substrate to tailor its surface properties (e.g., surface energy, dipole moment, and passivation) to cater to fundamental studies and applications spanning biosensing, nanotechnology, electronics, and photovoltaics.[1,2] SAMs can be coated onto diverse substrates with conformality to their surfaces. Coupled with their thin film nature, SAMs offer advantages in material consumption, light transparency, and charge carrier transfer. They also benefit from high molecular designability, mechanical flexibility, and compatibility with both solution and vacuum processing. Central to making the best use of SAMs is enhancement of packing density for high surface coverage and designing functional groups for effective interface interaction and energy level alignment with the active layer while ensuring strong chemical adsorption to substrates.

The rapidly growing use of SAMs has become notable in the research of lead halide-based perovskite solar cells (Pb PSCs). High performance is achieved with the SAM, whose molecules embed carbazole moieties, as used as a hole selective layer (HSL) in a p-i-n device architecture. Recently, SAMs have been instrumental in setting performance records for PSCs. For example, the all-time high efficiency (>26%) of power conversion (PCE), along with the maximum power point (MPP) tracking stability (T_{95} of 1,200 h, where T_{95} represents the time required to retain 95% of the initial efficiency), has been reported.[3] Moreover, high efficiency of >33% is marked by the SAM in Si/perovskite tandem cells.[4] The high device performance primarily results from the SAM's ability to build an interface with the HSL, minimizing losses in photovoltaic properties and avoiding dopants that could undermine stability. Alongside parallel research on perovskites and electron-selective layers (ESLs), SAM research is anticipated to bring further compelling progress for Pb PSCs in the near future.

Unfortunately, the aforementioned performance has not yet been attained by other types of prospective PSCs, namely, the Sn−Pb and Sn PSCs. Both types of devices hold smaller bandgap energies (below 1.5 eV) than the Pb PSC, which theoretically allows for greater efficiency. As a result, the Sn−Pb PSC serves as a narrow bandgap subcell in perovskite/

Received: November 20, 2024
Revised: January 14, 2025
Accepted: January 27, 2025

https://doi.org/10.1021/acsenergylett.4c03228
ACS Energy Lett. 2025, 10, 1292−1312

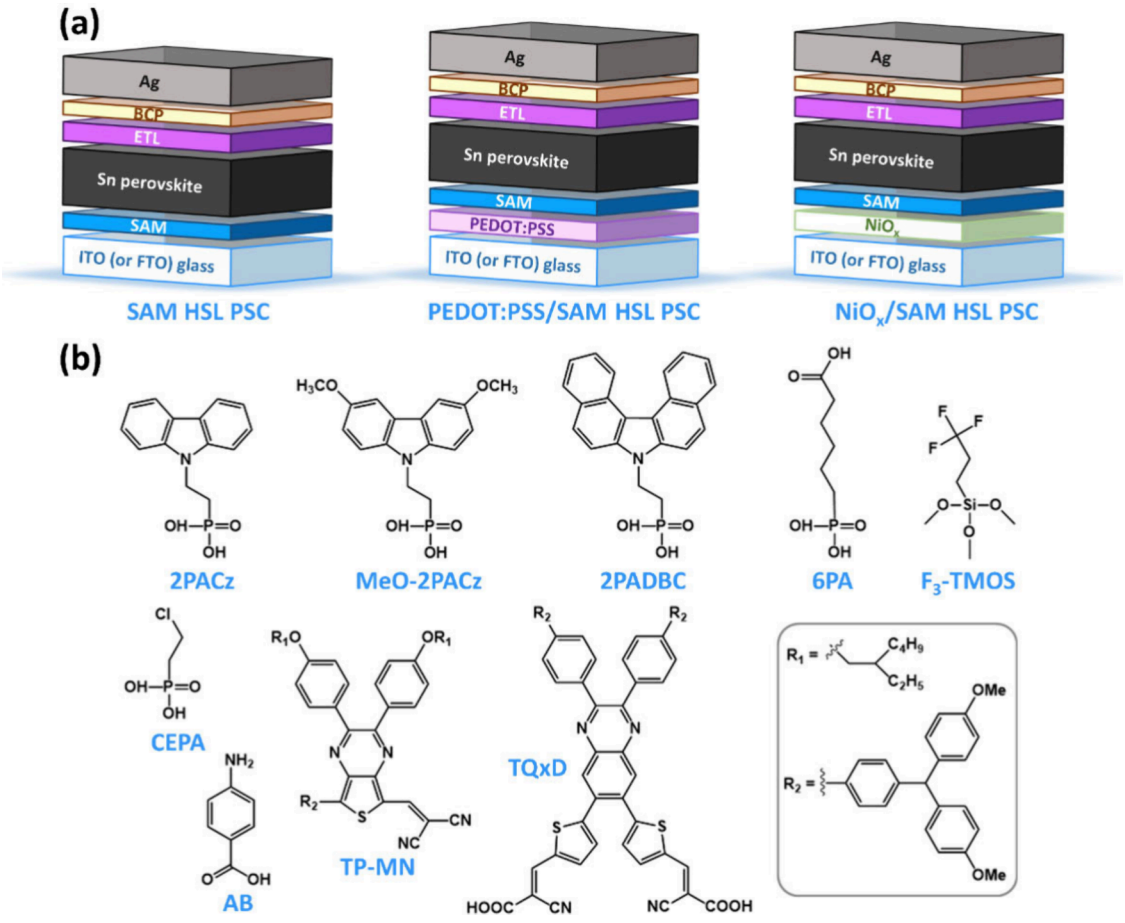

Figure 1. (a) Schematic illustrations of three different types of Sn PSCs utilizing SAM only, PEDOT:PSS/SAM, and NiO_x/SAM HSLs where BCP represents bathocuproine. (b) Representative SAM molecules used for Sn PSCs, with the R_1 and R_2 functional groups in TP-MN and TQxD highlighted in a rounded rectangle. The full names of the SAM molecules are as follows: [2-(9H-carbazol-9-yl)ethyl]phosphonic acid (2PACz), [2-(3,6-dimethoxy-9Hcarbazol-9-yl)ethyl]phosphonic acid (MeO-2PACz), (4-(7H-dibenzo[c,g]carbazol-7-yl)ethyl)phosphonic acid (2PADBC), 6-phosphonohexanoic acid (6PA), trimethoxy (3,3,3-trifluoropropyl)-silane (F_3-TMOS), 2-chloroethylphosphonic acid (CEPA), 4-aminobenzoic acid (AB), 2-((7-(4-(bis(4-methoxyphenyl)amino)phenyl)-2,3-bis(4-((2-ethylhexyl)oxy)phenyl)thieno[3,4-*b*]-pyrazin-5-yl)methylene)malononitrile (TP-MN), and (2E,2′E)-3,3′-((2,3-bis(4′-(bis(4-methoxyphenyl)amino)-[1,1′-biphenyl]-4-yl)-quinoxaline 6,7-diyl)bis(thiophene-5,2-diyl))bis(2-cyanoacrylic acid) (TQxD).

perovskite tandem cells and is responsive to light at relatively long wavelengths (up to ∼1,000 nm). The Sn PSC benefits from high carrier mobility, slow cooling of hot carriers, relative broad light harvesting (wavelength: up to ∼900 nm), and sustainability.[5] The wide bandgap (>1.6 eV) Sn PSC seeks applications like Si/perovskite tandem cells with sustainability.[6,7] Meanwhile, the hitherto high efficiency of the Sn−Pb PSC using a SAM HSL exceeds 23%,[8,9] which is impressive and approaching that of the Pb PSC. In contrast, the best Sn PSC using a SAM HSL attains 9.6% efficiency[10] and that using two HSLs of PEDOT:PSS/SAM, where PEDOT:PSS is the poly(3,4-ethylenedioxythiophene) polystyrenesulfonate, exhibits efficiency 14.67% and N_2-shelf storage lifetime ($T_{\sim 90}$ for 1000 h).[11] Using two HSLs of nickel oxide (NiO_x)/SAM, the high efficiency (14.19%) and stability (T_{93} for 1000 h) was recently reported.[18] Even though the SAM-based Sn PSCs are significantly underdeveloped relative to the Pb and Sn−Pb counterparts, their recent advancements that have closed the gap with the best Sn PSC based on a HSL of PEDOT:PSS presenting 15.7% efficiency[12] should encourage compelling future research efforts.

Specifically, we elaborate on potential merits of using two HSLs of PEDOT:PSS/SAM and NiO_x/SAM. As SAMs are deposited onto substrates such as indium tin oxide (ITO) glass, their coverage may not always be perfect to spoil the interface with perovskite due to factors such as aggregation of SAM molecules and imperfections of the ITO surface. On the other hand, PEDOT:PSS suffers from hygroscopic nature and fast recombination and NiO_x contains reactive species of $Ni^{\geq 3+}$ and exhibits relatively low reproducibility.[13] The two HSLs can overcome the respective limitations inherent in each individual HSL. In addition, they could effectively extract hole charge carriers by a cascade-like transfer. They also allow for tuning of the interface properties: for example, PEDOT:PSS enables smooth surface and is soft adaptable to perovskite lattice expansion and shrinkage under stress conditions: nanocrystalline NiO_x facilitates a flatter surface on the ITO substrate and homogeneous distribution of SAM molecules.[13−15] However, it needs to be remarked that a SAM sole HSL could be improved in the aforementioned interfacial properties, as well as surface coverage. We thus believe that advancing both HSL systems in parallel is required to make a breakthrough in the Sn PSC research.

Herein, we look at the so-far progress of Sn PSCs using SAM HSLs from 11 research papers.[6,7,10,11,14,16−21] We then review multifaceted approaches on SAM HSLs made for high-

https://doi.org/10.1021/acsenergylett.4c03228
ACS Energy Lett. 2025, 10, 1292−1312

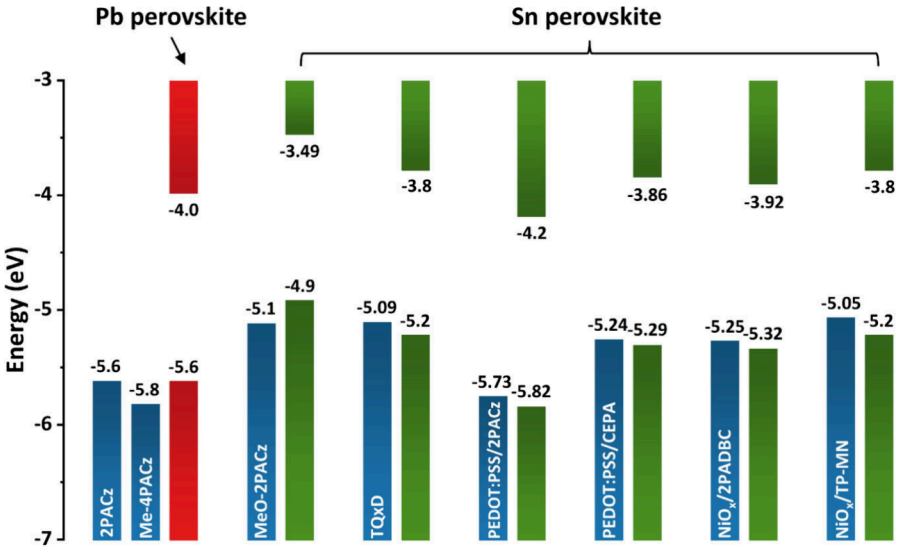

Figure 2. Energy level diagrams of SAM, PEDOT:PSS/SAM, and NiO_x/SAM HSLs in Sn PSCs are presented in which the HOMO energy level of PEDOT:PSS/CEPA is derived from PEDOT:PSS. For comparison, representative SAMs of 2PACz and Me-4PACz, known for high-performance in Pb PSCs, are also included. All data are sourced from Table 1, except for the Pb perovskite energy levels.[23]

performance Pb or Sn−Pb PSCs, by which the remaining challenges and strategies for Sn PSCs are identified and discussed. Since not all issues are addressable by this literature review due to unique properties of Sn perovskite, we further suggest our perspective on these properties to tackle the challenges.

SAM HSL RESEARCH IN SN PSCS

Characteristic Features of Functional Groups in SAM Molecules. Inverted architecture, specifically p-i-n, is predominantly used for high-performance, where a HSL plays a pivotal dual role in extracting holes and regulating perovskite quality. SAMs have been explored by one of three HSL structures: SAM, PEDOT:PSS/SAM, and NiO_x/SAM. As a substrate, either ITO glass (mostly) or FTO glass is typically used. Sketches of the full device structures are presented in Figure 1a and representative SAM molecules are added in Figure 1b. In general, SAMs consist of three functional parts that include a terminal group, a spacer group, and an anchoring group. The anchoring group ensures that SAM is firmly attached to the substrate via chemical (and/or physical) linkage. The so-far used anchoring groups include phosphonic acid (for 2PACz, MeO-2PACz, 2PADBC, 6PA, and CEPA), carboxylic acid (AB), silane (F_3-TMOS), cyanoacrylic acid (TQxD), and dicyano vinylene (TP-MN). These anchoring groups have different binding energies and modes.[1] Phosphonic acid groups are an excellent choice because they suppress homocondensation (i.e., polymerization), are compatible with various oxide substrates, including ITO and FTO glass substrates, and bind firmly to the substrates. In addition, they offer high surface loading and hydrolytic stability. Using two anchoring groups in a single SAM molecule (TQxD) could attain stronger binding. Silane groups are initially hydrolyzed, for example, by surface water and then covalently bind to the substrates. It is known that silane-based SAM molecules can polymerize while binding to the substrates with polymerization accelerated in the presence of excess water.

The spacer group bridges the terminal and anchoring groups. As exemplified in Figure 1b, two types of spacer groups are employed, nonconjugated (e.g., aliphatic chains) and conjugated groups (e.g., aromatic rings). AB, TP-MN, and TQxD SAM molecules have conjugated spacer groups, while the others use nonconjugated spacer groups consisting of aliphatic chains. The spacer group influences on charge selectivity, and at the same time, aids self-assembly through dipole−dipole, $\pi-\pi$, and CH−π interactions and van der Waals forces. Conjugated spacer groups allow charge delocalization, contributing to improved stability. In contrast, aliphatic chains contribute to charge carrier separation, physical barrier formation, and SAM molecule solubility. We further note that long aliphatic chains could undermine the tunneling of hole charge carriers, and on the other hand, are flexible and undergo van der Waals interaction to control the SAM orientation and interface quality,[22] so designing an appropriate length of aliphatic spacer is pivotal.

The terminal group primarily determines the functionality and interface (or surface) properties such as the dipole moment, packing, and orientation of SAM molecules, as well as interfacial defects. Moreover, it influences the perovskite crystal quality. The SAM molecules in Figure 1b feature core moieties of carbazole groups (2PACz, MeO-2PACz, and 2PADBC), a phenylene group (AB), thienopyrazines (TP-MN), a quinoxaline group (TQxD), and aliphatic groups (6PA, F_3-TMOS, and CEPA). Incorporating electron rich groups, including carbazole and triphenylamine, can promote hole selection, as corroborated by high-efficiency Pb PSCs. Introducing a phenoxy group in TP-MN can suppress the aggregation of SAM molecules, while the addition of a 4,4′-dimethoxytriphenylamine group in TP-MN and TQxD can increase their solubility in organic solvents. Dangling moieties of methoxy (MeO-2PACz and TQxD), carboxylic acid (6PA), amine (AB), chloride (CEPA), and fluorine (F_3-TMOS) groups can form hydrogen, halogen, or coordination bonds with perovskite, the chemical interaction facilitating stable interface formation. These moieties such as methoxy and amine groups and carboxylic acid can lower the contact angles (CAs) of perovskite precursor solutions (or water), which is conducive to the lamination of perovskite films onto SAMs in accordance with the Young−Dupré equation:

https://doi.org/10.1021/acsenergylett.4c03228
ACS Energy Lett. 2025, 10, 1292−1312

$$W_a = \sigma_l(1 + \cos\theta) \quad (1)$$

where W_a, σ_l, and θ stand for the work of adhesion, the surface tension of the perovskite solution, and the CA.

While the dipole moments of SAM molecules are influenced by all functional groups, they can be modulated by the type and position of the dangling moieties, thereby altering the work function (WF) of substrates and the highest occupied molecular orbital (HOMO) energy levels of SAMs; all data on the SAM-based Sn PSCs are summarized in Supporting Information. This is exemplified by the WF that is reduced from +2 D for 2PACz to +0.2 D for MeO-2PACz with the methoxy moieties.[23] Additionally, 2PADBC adopting a helical π-extension on the carbazole moiety increases its dipole moment from +2.13 D to +2.71 D compared to the parent molecule of 2PACz.[20] Figure 2 presents energy level diagrams displaying the HOMO energy levels of SAM, PEDOT:PSS/SAM, and NiO_x/SAM HSLs used for Sn PSCs, along with the energy levels of Sn perovskites. Overall, the energy level offsets between the HSLs and Sn perovskites are small ($\leq$0.2 eV). And, the HOMO energy levels are noticeably elevated, likely to align with Sn perovskites with narrow bandgaps ($\sim$1.4 eV) whose valence band maximum (VBM) energy levels are relatively shallow; for comparison, the energy levels of HSLs and Pb perovskites are also presented in Figure 2. We further need to remark that, in addition to modulating energetic properties, dipole moment affects not only self-assembly and coverage of the SAM but also SAM/perovskite interface passivation by protecting undercoordinated perovskite species and/or repelling electrons.

It is worthwhile mentioning that beyond those presented in Figure 1b, all functional groups in SAM molecules are tailorable for Sn perovskites to achieve target properties mentioned above due to the high molecular tunability afforded by the extensive library of organic compounds.

Photovoltaic Performance with SAMs. While discussing the properties of SAM molecules themselves above, we now turn to their effects on device performance in Sn PSCs. The first use of SAMs as a sole HSL in Sn PSCs was reported in 2021.[16] In this study, three SAM molecules −2PACz, MeO-2PACz, and Me-4PACz were tested by a dipping method for Sn PSCs. These molecules are commercially available and have demonstrated high-performance in Pb and Sn−Pb PSCs. They all feature a carbazole core that is bridged by an ethyl chain for 2PACz and MeO-2PACz (or a butyl chain for Me-4PACz) to an anchor of phosphonic acid. Additionally, MeO-2PACz and Me-4PACz have methoxy and methyl groups at the 3,6 positions, respectively. Among these, MeO-2PACz, which is the most hydrophilic, possesses a shallow HOMO energy level along with an interactive methoxy terminal group, marked the highest efficiency (4.1%) according to a two-step fabrication process to make the tin perovskite layer. In contrast, Sn perovskite films were difficult to form on the Me-4PACz. Interestingly, it was discovered that the hydrophilicity was strengthened for better formation of perovskites and remaining layers, resulting in the increased J_{SC} and PCE to 20.3 mA cm^{-2} and 6.5%, respectively, as ITO glass substrates were annealed at 400 °C for 30 min. The impressive stability is manifested as a T_{80} lifetime of $\sim$1,900 h under shelf-storage in a N_2-filled glovebox.

Overall, adopting a two-step deposition method for Sn perovskites is crucial regardless of the SAM type. This method involves sequential spin-coating of the SnI_2 dissolved dimethyl sulfoxide (DMSO) precursor solution and the FAI precursor solution. When using a one-step deposition of Sn perovskite, the MeO-2PACz SAM shows potential as an efficient HSL in Sn PSCs, as highlighted in recent reports.[10,18] Notably one report describes a holistic approach entailing comolecular SAMs, perovskite engineering, and an efficient ESL (indene-C60 bisadduct, ICBA) to decline photovoltage deficit.[10] The comolecular SAM is composed of MeO-2PACz and 6PA molecules of complementary properties: incorporating the 6PA molecule−featured as a hydrocarbon chain core bridging a phosphonic acid anchoring group and a carboxylic acid terminal group−is effective for perovskite lamination, enabling high open-circuit voltage (V_{OC}) of 0.829 V and a PCE of 9.4%, the best among SAM only HSL-based Sn PSCs. As assessed by the CA measurements, it turns out that 6PA had higher surface energy than MeO-2PACz due to the $\sim$2.5-fold greater polar components for hydrogen bonds and ion-dipole interactions. Interestingly, it is found that perovskite film thickness is sensitive to the precursor solution volume, unlike PEDOT:PSS, inviting eclectic engineering efforts on the comolecular ratio, perovskite precursor volume, and even antisolvent volume and type.[10]

In another report, solvent engineering on superseding the common solvent (DMSO) of with *N*,*N*-diethylformamide/*N*,*N*′-dimethylpropyleneurea (DEF/DMPU) was employed to attain 5.8% device efficiency.[18] The justification of selecting DMSO-free solvent comes from the fact that DMSO acts as an oxidizer for Sn(II) in the perovskite solution and is partially reduced to dimethyl sulfide with room for impinging on the crystallization rate. Meanwhile, the MeO-2PACz SAM was deposited by spin-coating at rates ranging from 4000 to 6000 rpm. Interestingly, the highest rate presumably leading to the thinnest SAM film resulted in the smallest water CA (55.39 → 47.07°) and highest average efficiency. As the MeO-2PACz SAM is compared with a PEDOT/Al_2O_3 HSL at the device level, a higher V_{OC} (0.590 → 0.638 V at the reverse J−V scan) and a narrower hysteresis index distribution are observed in the J−V curves.

Besides the aforementioned carbazole-based molecules, other promising SAM molecules have been successfully developed for Sn PSCs. The TQxD SAM molecule embeds 4,4′-dimethoxytriphenylamine groups to effectively donate electrons to perovskites and two anchoring groups for strong binding.[17] It also features a dye molecular structure incorporating conjugated spacers. The thiophene group attached to the core quinoxaline moiety plays a crucial role in forming perovskites with excellent crystal quality. The TQxD SAM afforded the proper energy level of HOMO (−5.09 eV) and led to improved efficiency to 8.3%, accompanied by a lifespan exceeding 1,600 h of T_{80}. The AB SAM molecule is designed with a phenylene core that bridges an electron-withdrawing carboxylic acid group and an electron-donating amine group, resembling an acceptor-π-donor configuration.[21] Rather than phosphonic acid, carboxylic acid was chosen due to the higher reactivity with preferred adsorption to the ITO glass substrate. The AB SAM exhibits excellent wettability with the precursor solution, as indicated by a small CA of 6.52°. Notably, the perovskite precursor solutions present smaller CAs than water (see Supporting Information), on the back of decreased surface tension. The decent device efficiency (7.6%) and stability (3,500 h of T_{80}) were recorded. As compared with PEDOT:PSS which is currently the most efficient HSL for Sn PSCs, the AB SAM

https://doi.org/10.1021/acsenergylett.4c03228
ACS Energy Lett. 2025, 10, 1292−1312

Table 1. Summary of key properties of hole-selective SAM-based Sn PSCs, including the photovoltaic parameters presented in Figure 3

	HSL			Perovskite			Device						
	Substrate WF (eV)	E_{HOMO} (or E_{VBM}) (eV)	CA (deg)	Deposition	E_g (eV)	E_{VBM} (eV)	Structure	V_{OC} (V)	J_{SC} (mA cm^{-2})	FF(%)	PCE(%)	Year	ref.
MeO-2PACz[1]	4.6[a]	−5.1	55[a]	2-step method	1.41[c]	−4.9	ITO/SAM/Perovskite/C60/BCP/Ag	0.474	20.3	67.7	6.5	2021	16
TQxD	4.115	−5.09	19.4[b]	2-step method	1.4	−5.2	ITO/SAM/Perovskite/C60/BCP/Ag	0.574	21.05	68.8	8.3	2023	17
AB	4.8	-	6.52[b]	2-step method	1.4	−5	ITO/SAM/Perovskite/C60/BCP/Ag	0.534	19.92	71.9	7.6	2023	21
MeO-2PACz[2]	-	−5.3	47.07[a]	1-step method	1.4	−4.9	ITO/SAM/Perovskite/C60/BCP/Ag	0.638	14.3	64	5.8	2023	18
MeO-2PACz:6PA	-	-	-	1-step method	1.43[c]	-	ITO/SAM/Perovskite/ICBA/BCP/Ag	0.829	17.6	64.5	9.4	2024	10
PEDOT:PSS/2PACz	4.7	−5.73	-	1-step method	1.62	−5.82	FTO/PEDOT:PSS/SAM/Perovskite/C60/BCP/Ag	0.73	16.28	72	8.62	2022	6
PEDOT:PSS/MeO-2PACz	4.9	-	-	1-step method	1.66	−5.31	ITO/PEDOT:PSS/SAM/Perovskite/PCBM/BCP/Ag	0.91	16.23	77.56	11.5	2023	7
PEDOT:PSS/F_3-TMOS	-	-	-	1-step method	1.43[d]	-	FTO/PEDOT:PSS/SAM/Perovskite/ICBA/BCP/Ag	0.91	22.52	71.56	14.67	2024	11
PEDOT:PSS/CEPA	4.7	−5.24	38[a]	1-step method	1.43[d]	−5.29	ITO/PEDOT:PSS/SAM/Perovskite/C60/BCP/Ag	0.64	23.17	71.81	10.65	2024	19
NiO_x/2PADBC	-	−5.25	-	1-step method	1.4[c]	−5.32	ITO/NiOx/SAM/Perovskite/C60/BCP/Ag	0.825	23.23	74.06	14.19	2024	20
NiO_x/TP-MN	4.7	−5.05	12.31[b]	2-step method	1.4	−5.2	ITO/NiOx/SAM/Perovskite/C60/BCP/Ag	0.56	19.28	71	7.7	2024	14

[a]Measured by DI water. [b]Measured by the perovskite precursor. [c]Approximated by the absorption spectra. [d]Approximated by the photoluminescence spectra.

https://doi.org/10.1021/acsenergylett.4c03228
ACS Energy Lett. 2025, 10, 1292−1312

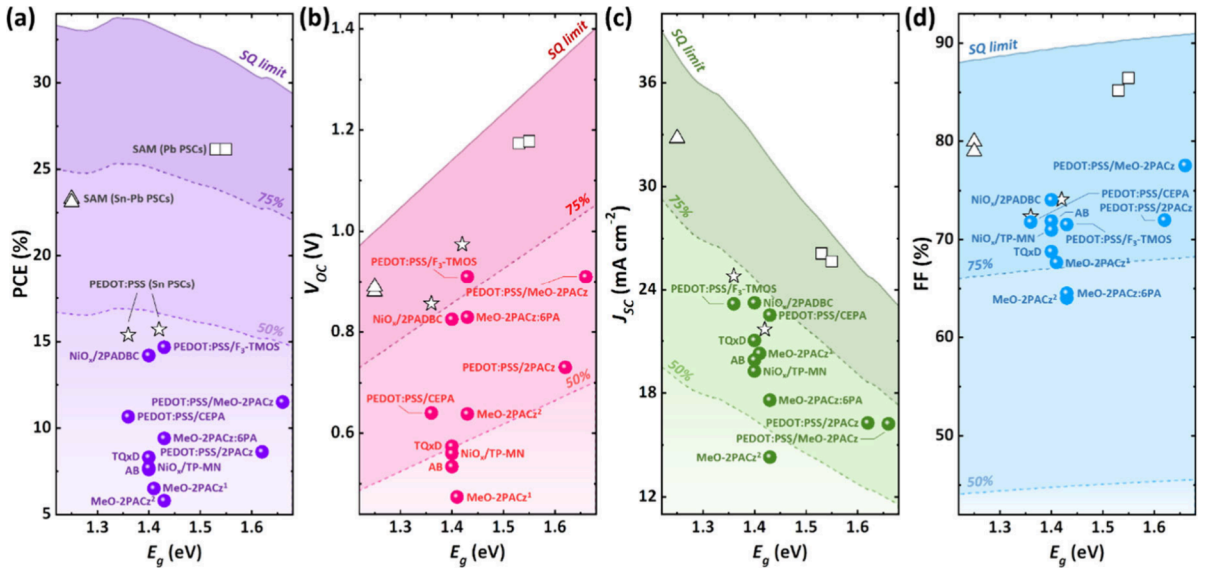

Figure 3. Bandgap-dependent photovoltaic parameters, (a) PCE, (b) V_{OC}, (c) J_{SC}, and (d) FF of Sn PSCs incorporating SAM HSLs, with numerical values presented in Table 1. For comparison, high-efficiency Pb and Sn−Pb devices using SAM HSLs and Sn PSCs with a PEDOT:PSS HSL are inserted. The SQ limit, along with its 75% and 50% thresholds, is added as a reference.

attains higher stability under ambient conditions (relative humidity: 60%) without encapsulation.

The TP-MN SAM molecule is an organic dye based on a thienopyrazine core moiety that is conjugated with a dicyano vinylene anchoring group on one end and attaches the 4,4′-dimethoxytriphenylamine group (for electron donation to perovskite) and a phenoxy group (for dye dispersal) on the other end.[14] The TP-MN SAM is decorated atop a NiO_x nanoparticulate film on an ITO glass substrate to form the NiO_x/SAM HSL; we note that the TP-MN SAM with a cyano anchoring group could adsorb onto NiO_x as other anchoring groups do, enabling its deposition using the same methods, such as spin-coating and dipping, applied to ITO and FTO substrates. It is claimed that NiO_x reduces the substrate roughness and provides a higher density of hydroxyl groups for SAM anchoring compared to ITO. However, NiO_x is susceptible to forming oxygen vacancies to react with tin iodides (i.e., $SnI_2 \rightarrow SnI_4$) upon contact with Sn perovskite. The TP-MN SAM with the 4,4′-dimethoxytriphenylamine group helps to prevent this reaction. In addition, the TP-MN SAM resulted in the formation of a ∼ 2-fold thicker perovskite film with large crystal grains together with an appropriate energy level of VBM (−5.05 eV). The decent device efficiency (7.7%) and stability (4,000 h for $T_{\sim 80}$) are accompanied as a result.

The two-step deposition method for perovskite has been primarily applied to SAM-only HSLs while the one-step method has been mostly used with SAM HSLs on NiO_x or PEDOT:PSS (see Table 1). The one-step method can be advantageous for engineering high quality perovskite crystals. 2PADBC is a high-performance SAM whose molecule contains a π scaffold of 7H-dibenzo[c,g]carbazole core with a hydrocarbon spacer group and a phosphonic acid anchoring group.[20] Especially, the π scaffold renders a helical π-extension that can promote self-assembly by increasing both the dipole moment and $\pi-\pi$ interactions as compared to the mother molecule of 2PACz. According to the differential charge density simulation, the increased dipole moment could populate electron density near Sn atom to suppress its oxidation. 2PADBC is specifically effective as used onto a NiO_x HSL as it passivates and homogenizes the surface. Following the dipole moment strength, the VBM energy level of NiO_x/2PADBC is slightly lowered by 0.1 eV, to −5.25 eV, relative to that of NiO_x/2PACz. With the NiO_x/2PADBC HSLs, Sn PSCs attain the high J_{SC} of 23.23 mA cm^{-2} and PCE of 14.19%, along with the stability of 1,000 h of T_{93}. Under thermal stress at 85 °C in a nitrogen environment, the thermal stability was impressive, with a $T_{\sim 90}$ lifetime of 500 h. While thermal stability is not frequently reported in Sn PSCs, this result is encouraging. Even after scaling the active area from 0.04 to 1.00 cm^2, the PCE remains high at 12.05%.

In addition to the NiO_x scaffold, PEDOT:PSS has been used in conjunction with several SAM molecules; it should be noted that PEDOT:PSS could be dissolved in SAM processing solvents at varying rates; therefore, its processing predominantly involves spin-coating, which has a shorter processing time than dipping. Even though PEDOT:PSS proves effective for high-performance Sn PSCs, it is hygroscopic and acidic likely being detrimental over long periods of operation. Introducing the 2PACz SAM atop PEDOT:PSS would mitigate this issue.[6] It is claimed that 2PACz molecules anchor to PEDOT:PSS via ionic interactions between the P−O$^-$ groups of 2PACz and the S$^+$ groups of PEDOT, creating a thin monolayer (sub 1 nm). The PEDOT:PSS/2PACz HSL effectively suppresses Sn oxidation and eliminates lattice strain in the perovskite crystals. The measured VBM energy level of −5.73 eV is deeper than that of PEDOT:PSS by 0.6 eV. This energy level is compatible with the wide bandgap perovskite used in this research. As a result, a PCE of 8.66% and FF of 73%, which are decent for wide bandgap devices, are yielded. The stability includes a T_{75} lifetime of 70 days under shelf-storage in a nitrogen atmosphere, and a T_{70} lifetime of 70 min at 85 °C temperature in the ambient atmosphere. The MeO-2PACz SAM has been also coupled with PEDOT:PSS in Sn PSCs, attaining a PCE of 12.16% with reduced $J-V$ hysteresis and a N_2 shelf storage stability (>2,000 h of T_{100}).[7] The origin of the reported performance comes from the MeO-2PACz insertion improving interfacial properties toward reducing

https://doi.org/10.1021/acsenergylett.4c03228
ACS Energy Lett. 2025, 10, 1292−1312

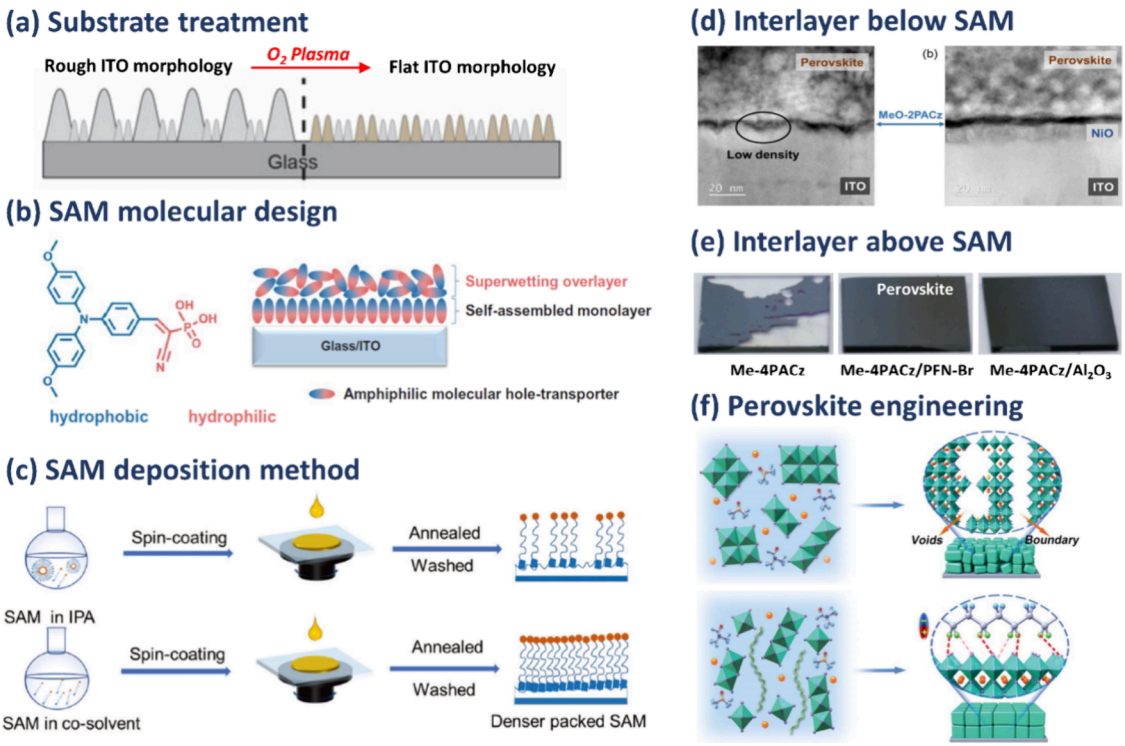

Figure 4. Representative examples of key approaches used for Pb PSCs. (a) Schematic diagram of the ITO substrate morphology before and after plasma treatment. The brown color indicates the spike shape ITO morphology is modified to a flatter ITO morphology after plasma treatment.[30] Reproduced with permission from Wiley-VCH, Copyright 2023. (b) Molecular structure of the amphiphilic MPA-CPA molecule and schematic depiction of the bilayer stack of MPA-CPA molecules on an ITO-glass substrate.[33] Reproduced with permission from American Association for the Advancement of Science, Copyright 2023. (c) Schematic diagram for SAMs deposited from IPA or cosolvent.[34] Reproduced with permission from Wiley-VCH, Copyright 2023. (d) High-angle annular dark-field images of a cross section of the ITO/MeO-2PACz device (left) and ITO/NiO + MeO-2PACz device (right).[15] Reproduced with permission from American Chemical Society, Copyright 2021. (e) Photographs showing the poor wettability of perovskite on bare Me-4PACz which is significantly improved upon modification with PFN-Br and Al_2O_3.[35] Reproduced with permission from Wiley-VCH, Copyright 2023. (f) Schematic of processing control (top) and target (bottom) perovskites.[36] Reproduced with permission from American Association for the Advancement of Science, Copyright 2023.

defects, suppressing Sn oxidation, and enhancing perovskite quality in terms of crystallinity and orientation.

The CEPA SAM molecule, containing a hydrocarbon chain between a chloride terminal group and a phosphonic acid anchoring group, was also applied to PEDOT:PSS.[19] The chloride terminal group is disclosed to be interactive with the major perovskite precursor (SnI_2). This not only removes excess PSS and passivates the interface with perovskite but also lowers the VBM energy level (−5.09 → −5.24 eV) toward minimizing the energy offset. In addition, it regulates perovskite crystals for improving crystallinity while suppressing defects of the oxidized tin, iodine, and voids. As a consequence, the PEDOT:PSS/CEPA SAM enabled the Sn PSC to achieve J_{SC} of 23.17 mA cm^{-2}, FF of 71.81%, and a PCE of 10.65%. The shelf-storage stability (850 h of T_{80}) and light aging stability of (240 h of T_{80}) were attendant, both assessed in an N_2 environment. Meanwhile, the F_3-TMOS SAM molecule was introduced on top of PEDOT:PSS.[11] It embeds a hydrocarbon chain with rimethoxysilane anchoring and CF_3 terminal groups. Unlike phosphonic acid, silane must undergo hydrolysis for heterocondensation (for anchoring to the substrate) and homocondensation (for polymerization of the molecules). The CF_3 group, being electron-withdrawing, contrasts with the electron-donating NH_2 group. The PEDOT:PSS WF is increased by the CF_3 group, which is opposed by the NH_2 group, in relation to the dipole moment. This WF alteration indicates that the CF_3 group is relatively electronegative, making dipole points away from the substrate, whereas the NH_2 group is relatively electropositive, creating dipole points toward the substrate. It is claimed that the increased WF is favorable for hole extraction from the perovskite. The F_3-TMOS surface modification reinforces Sn perovskite film formation by facilitating higher crystallinity and crystal orientation, attenuating defects, and alleviating interfacial strain and distortion. Consequently, a high PCE (14.67%) owing to the V_{OC} (0.91 V), J_{SC} (22.52 mA cm^{-2}), and FF (71.56%) was reached.

Performance Comparison of SAM HSL-Based PSCs. In Figure 3 and Table 1, we summarize photovoltaic parameters (PCE, V_{OC}, J_{SC}, and FF) of the aforementioned Sn PSCs with SAM HSLs as a function of perovskite bandgap energy (E_g) for comparative analysis. The Shockley-Queisser (SQ) limit, along with its 75% and 50% thresholds, is presented as a guide. The SQ limit sets the upper boundaries for the photovoltaic parameters. For broader insights, the high-performance SAM-based Pb and Sn−Pb PSCs,[3,8,9,24] as well as PEDOT:PSS-based Sn PSCs[12,25] are also included in Figure 3. Above all, the PCE presented in Figure 3a points to that the Pb PSCs are above the 75% limit with offsets of 5.35−5.68% from the SQ limit and the Sn−Pb PSCs are approaching this limit, with offsets of 9.81−10.01% while the Sn PSCs reside below the 50% limit with offsets of 17.52−18.34% for PEDOT:PSS and >

https://doi.org/10.1021/acsenergylett.4c03228
ACS Energy Lett. 2025, 10, 1292−1312

~20% for SAMs. Despite having lower SQ limits due to larger bandgaps, the supreme PCEs are recorded by the Pb PSCs, accounted for by the highest photovoltaic parameters far above the 75% limit, as shown in Figures 2b-d. They are a consequence of well-developments of perovskites, contact materials, and deposition methods, for which many worldwide researchers have strived. The Sn−Pb PSCs are fairly mature and close the performance gap with the Pb PSCs. In stark contrast, the Sn PSCs incorporating PEDOT:PSS and SAM HSLs leave abundant room for improvement, despite the potential for higher efficiency.

Overall, the data points of the photovoltaic parameters of the SAM-based Sn PSCs are scattered due to ongoing development since their introduction in late 2021 and the V_{OC} and J_{SC} values are largely spread below the 75% limit, whereas the FF values remain above this threshold with smaller deviations, albeit with a few exceptions. The two devices of PEDOT:PSS/2PACz and PEDOT:PSS/MeO-2PACz utilize wide bandgap (>1.6 eV) Sn perovskites. Interestingly, it is observed that J_{SC} is the least developed even in the PEDOT:PSS devices. The SAM-based Sn PSCs attaining a PCE over 14% typically incorporate either PEDOT:PSS/F_3-TMOS or NiO_x/2PADBC, exhibiting photovoltaic parameters that are mostly greater than the SAM-only (below 10%). The >14% devices are not the best-efficiency Sn PSCs. These contradict with the Pb PSCs reaching high efficiency with SAM-only HSLs. Importantly, comparative studies to understand the fundamentals of the aforementioned trends are deficient for SAM-based Sn PSCs. In the following paragraphs, we explore the strategies developed for SAM HSLs in Pb and Sn−Pb PSCs aiming to draw valuable insights and explore how to apply them to Sn PSCs. We categorize the strategies used in SAM-based Pb and Sn−Pb PSCs into five sectors: the substrate treatment, SAM deposition, SAM molecular design, overlayers, and perovskite engineering. Furthermore, given the unique properties of Sn perovskites, we propose additional insights to consider to expand on the strategies gained from Pb and Sn−Pb PSCs.

LITERATURE SURVEY ON PB OR SN−PB PSCS USING SAM HSLS

Brief Introduction. In the pioneering research reported in 2018 on a SAM HSL based on carbazole-based molecule (called V1034), a respectable PCE of 17.8% was achieved for a Pb PSC, which had only a gap of ~5% compared to the certified best PSC at the time.[26,27] Then, the next generation of carbazole-based molecules of 2PACz, MeO-2PACz, and Me-4PACz were disclosed,[22,23] and these have been commercialized and frequently used due to their high performance and reproducibility. The advent of these SAM molecules (particularly, Me-4PACz) has advanced the development of tandem solar cells, exemplified by the c-Si/PSC.[22] The success of these SAMs stems from the fact that PSCs were already fairly well-developed at the moment in light of perovskite film formation and contact materials (including ESLs and metals). Since then, multifaceted approaches involving substrate treatment, SAM molecular design and deposition methods, interlayers, and perovskite engineering have led to present-day SAM HSL-based PSCs exceeding 26% (for Pb perovskite)[3,24] and 23% (for Sn−Pb perovskite)[8,9] in PCE. In the following subsections, we will discuss key lessons from these staggering PCE achievements.

Substrate Modification. We summarize several examples of the multifaceted approaches in Figure 4. As substrates for SAM, ITO and FTO glass substrates that are commercially available are commonly used, even with varied qualities. They differ in surface properties of texture, WF, and chemical composition. In a report comparing the two using the same SAM molecules, PCEs of 24.4% (ITO) and 22.7% (FTO) were reported.[28] However, the effects of the substrate on SAM formation and device performance have yet to be fully explored. Though, many researchers choose to use ITO substrate.[29] Using the ITO substrate, a UVO pretreatment proceeds to clean surface carbon atoms and to increase surface oxygen concentration as a strategy to improve wettability. O_2 plasma treatment provides a similar surface modification effect as the UVO treatment while also physically etching the surface (Figure 4a). Specifically, the latter enables flatter surface texture for SAM growth.[30] Meanwhile, ITO surface is tailorable in chemical composition, via the successive treatments of hydrofluoric acid and UVO.[31] This, in turn, removes the undesired surface hydroxyls and hydrolyzed products and creates a partially fluorinated surface that improves interface passivation, reduces perovskite defects, and facilitates high-density SAM formation. It has been discovered that a significant amount of surface hydroxyls is weakly bound to the ITO surface to be washed away with ease by the perovskite precursor solvent.[32] For this reason, the ITO surface was reconstructed by implementing atomic layer deposition to form an ITO film with a thickness of ~9−10 nm. The similar surface reconstruction approach was reported for Sn PSCs, where annealing the ITO substrate at 400 °C modulated surface chemical composition toward effective SAM formation for Sn perovskites.[16]

SAM Molecular Design. *Anchoring Group.* Monopodal SAM molecules are exemplified by a series of carbazole-based compounds, 2PACz, MeO-2PACz, and Me-4PACz, each featuring a single anchoring group (phosphonic acid).[1] Meanwhile, several phosphonic acid-free anchoring groups have been designed, the examples of which are presented in the following. The acrylic acid that is a highly polar group is soluble in polar solvents like alcohols and the cyano group that can be categorized as a Lewis base group is capable of suppressing Pb^{2+} defects despite serving as an anchoring group.[37] Phosphonic acid in 2PACz has been replaced with carboxylic acid to create a new SAM molecule (9-carbazolyl)-acetic acid) while shortening the spacer group length.[38] This change in the anchoring group exerts influence on SAM orientation and arrangement for attenuated nonradiative recombination, improved perovskite crystallinity, and better energy level alignment and hence produces a high PCE (23.1%) and the shelf-storage lifetime (T_{93} for 2,500 h). Having the weaker acidity than phosphonic acid, boric acid was used as an anchoring group in a triphenylamine-based SAM molecule.[39] The boric-acid−based SAM can chemisorb to oxygen vacancy sites on the ITO surface. It is claimed that the weaker acidity mitigates ITO corrosion and enhances interface stability. Another SAM molecule with a trimethoxysilane group, (3,6-dimethoxy-9H-carbazol-9-yl)-trimethoxyphenylsilane, was synthesized.[32] The silane anchoring group presents greater binding energy (−6.94 → −14.65 eV), as calculated by the density functional theory (DFT), through the tridentate anchor mode, in contrast to the bidentate mode of phosphonic acid. In contrast, the multipodal SAM molecules possessing two or more anchoring groups

https://doi.org/10.1021/acsenergylett.4c03228
ACS Energy Lett. 2025, 10, 1292−1312

capable of stronger binding to substrates have been developed. The dipodal SAMs derived from indolocarbazole are designed with anchoring groups at three different positions (ortho, meta, para) of the two nitrogen atoms within the core unit.[40] The positioning of these anchoring groups affects the dipole moment and $\pi-\pi$ interactions, thereby regulating the interfacial properties. Tripodal monolayer molecules bearing triazatruxene core units were also designed.[41] In contrast to the edge-on orientation of monopodal SAM molecules, the tripodal molecules are subjected to the face-on orientation, which turns out to be effective for hole selection.

Spacer Group. [22] The aliphatic spacer in MeO-2PACz is replaced with a phenyl group which is more rigid and promotes intermolecular and intramolecular $\pi-\pi$ stacking and conjugation.[42] These molecular properties are translated into desired SAM characteristics for hole selection, nonradiative recombination, and UV light resistance. Meanwhile, adopting a phenyl spacer group could also strengthen the thermal stability. For instance, adding two phenyl groups in series raises decomposition temperature from 180 (for one phenyl group) to 354 °C according to thermogravimetry results.[43] As benzothiadiazole served as a spacer group, it strengthened structural planarity for intermolecular stacking and specific interactions between sulfur atoms and undercoordinated Pb^{2+} ions through coordination bonds.[37] A cyanovinyl spacer group can augment hydrophilicity greatly toward a super wettable surface to the perovskite precursor solution (CA: 4.9°) and demonstrate defect passivation capability via Pb−N interactions, as shown in the bilayer stack of SAM molecules (Figure 4b).[33]

Terminal Group. The so-far developed carbazole-based SAMs have several tail moieties including methoxy, methyl, phenyl, iodo, sulfur, methoxyphenyl, and dimethoxyphenyl groups.[22,23,44−47] The methoxy group bearing a Lewis basic heteroatom (i.e., oxygen) alters the dipole moment and passivates the perovskite surface by coordination with undercoordinated lead ions.[23] The dimethoxybenzene group reinforces energy alignment and solubility while promoting the formation of perovskite film with smoothness and compactness.[43] The methyl group that is weakly electron-donating affects energy alignment with the perovskite without significantly altering dipole moment and interface passivation.[22] The iodo group renders more wettable SAM surface, modifies dipole moment, and interacts with undercoordinated lead ion and with iodide and bromide ions by halogen bonding.[44] The phenyl groups expand the conjugation area, dipole moment, and dihedral angle, by which SAM solubility, energy level, and assembly along with perovskite crystallization can be ameliorated.[45,46] The sulfur group, with its Lewis basicity, can passivate undercoordinated lead ions; however, its controlled exposure, enabled by the methylation for steric hindrance, is crucial for adequate crystallization of perovskite.[47]

In place of carbazole, other core moieties such as triphenylamine,[33,37] zinc porphyrins,[48] a phenyl ring,[49] ruthenium(II) complex,[50] benzothiophene,[51] and tricyclic aromatic rings,[52] have been explored for SAM HSLs. In these carbazole-free SAMs, various tail moieties have been investigated. For instance, benzoic acid is para-substituted by $-NH_2$ (−4.5 D) < $-OCH_3$ (−3.9 D) < −H (−2.1 D) < −Cl (2.0 D) < −Br (2.1 D) for a wide range of dipole moments.[49] For the interaction with perovskite, hydrogen termination hinges on the van der Waals force, whereas the others do dipolar interactions. It was verified that perovskite crystallization is modulated by factors, such as the grain size, defect, and crystallinity. Meanwhile, heteroatoms of O, S, and Se are incorporated into SAM molecule based on tricyclic aromatic rings containing bromide groups as a core moiety.[52] While the bromide groups are especially electron-withdrawing for dipole moment control and electron blocking ability, the heteroatoms increase the interaction energy between the SAM and perovskite in the order Se > S > O, quantified by DFT calculations. This interaction plays a crucial role in vitiating interfacial defects and extending charge carrier lifetimes.

Comolecular SAM. Adopting comolecular SAMs comprising two or more different molecules of synergistic or complementary properties is an effective route to tailoring interfacial properties. As 1,6-hexylenediphosphonic acid is coassembled with Me-4PACz, the perovskite precursor solution wettability is enhanced, due to a ∼ 10% increased polar component of surface energy, to markedly promote lamination of the resulting perovskite film.[53] This concept was repeatable, as different types of perovskites and SAM molecules were tested. Meanwhile, interfacial passivation can be reinforced by coassembling (2,7-dimethoxy-9H-carbazol-9-yl)methyl) phosphonic acid and 6-(iodo-λ^5-azanyl) hexanoic acid onto an ITO substrate.[54] The former molecule is an analogy to MeO-2PACz and the latter molecule contains a linear alkyl chain capped with an ammonium group. Additionally, the latter molecule is greater in length than the former so as to make an ionic interaction with perovskite, thereby passivating the buried interface concurrently with maintaining efficient hole extraction. Methyl phosphonic acid coassembled with 2PACz for Sn−Pb PSCs attains high efficiency (23.3%) and improved thermal stability;[8] it is small in size and hence escalates the overall SAM coverage by anchoring onto exposed areas of the FTO substrate between 2PACz molecules. Energy level alignment between SAM and perovskite can be tuned by coassembling MeO-2PACz and 2PACz onto NiO_x.[55] The VBM energy levels are shiftable by approximately 0.6 eV between the upper limit (by MeO-2PACz) and the lower limit (by 2PACz). Meanwhile, Me-4PACz molecules are mixed with a polymer of PFN-Br (poly(9,9-bis(3′-(*N*,*N*-dimethyl)-*N*-ethylammonium-propyl-2,7-fluorene)-alt-2,7-(9,9-dioctylfluorene))dibromide) to create a more wettable surface.[56] The PFN-Br interacts with the A-site cation in perovskite so as to facilitate perovskite film formation with enhanced uniformity and crystallinity and, furthermore, improves energy level alignment with the perovskite.

Polymer SAM. New types of HSLs using polymerized SAM molecules have been reported. One promising example material is poly(carbazole phosphonic acid) which shows comparable hole transport capacity and solution processability.[57] It also shows lessened sensitivity to layer thickness and TCO roughness and passivates the interface with the perovskite. Consequently, the impressive device efficiency (24.4%) and MPP tracking stability (T_{94} of 1,500 h) are marked. Another example is based on poly(3-hexylthiophene) with carboxylic acid anchoring groups. This material yields a well-oriented polymer chain arrangement with a coil-like conformation.[58] It features a low-lying HOMO level, reduced surface defects, and low hydrophilicity (i.e., low surface energy) and enables perovskite to grow with a high degree of crystallinity; we specifically remark that the SAM surface energy could be in a trade-off relationship between perovskite wettability and crystallization. The polymer SAMs could affect

https://doi.org/10.1021/acsenergylett.4c03228
ACS Energy Lett. 2025, 10, 1292−1312

surface roughness and could be soft, adaptable to perovskite lattice change, which should be investigated in future research.

SAM Deposition Method. In addition to the substrate treatment and SAM molecular design, selecting and implementing an appropriate deposition method and conditions to attain the desired intermolecular packing and tight anchoring onto the substrate can be pivotal. Pretty manifold deposition methods are available and their SAM growth mechanisms are elaborated in the literature.[1,59] Spin-coating and dip-coating are mostly utilized, each with varied processing conditions.[60] For example, for the family of 2PACz, spin-coating employs a high concentration (∼ 1 mM) and a short processing time (spin-time: < 1 min) whereas dip-coating uses a relatively low concentration (e.g., ∼ 0.2 mM) and a long processing time (dipping-time: minutes-hours).[16,23] At high concentrations, SAM molecules would form micelles in the processing solution such as ethanol or isopropanol due to their amphiphilicity. By spin-coating that is kinetically driven with a short deposition time, the presence of micelles may suppress intermolecular packing. This issue can be mitigated by a cosolvent strategy (Figure 4c).[34] Adding dimethylformamide (DMF) as a cosolvent in 2-propanol (IPA) helps disassemble the SAM micelles by strong solvent−solute interactions with the carbazole group. The disassembled micelles ensure the improved packing density of SAM (2.48×10^{13} to 3.84×10^{13} molecules cm^{-2} evaluated from cyclic voltammetry) on the ITO substrate toward better energy level alignment, more efficient hole extraction, and attenuated interfacial recombination loss. Alternatively, by sequentially spin-coating the two different SAMs, the packing density can be increased.[61] Large-area applicability, process temperature controllability, and thermodynamically driven adsorption make dip-coating appealing. In particular, with the latter two, the SAM quality might differ from spin-coating depending on the types, solvents, and else.

In addition to spin- and dip-coating, other methods have been developed for SAM deposition. Spray-coating, a high throughput technique with unparalleled linear deposition speeds of up to 12 m min^{-1} was applied to deposit the MeO-2PACz SAM.[62] By comparison with other deposition methods including spin-coating, dip-coating, and airbrush-coating, it is disclosed that spray-coating can demonstrate a competitive PCE. Codeposition represents the concurrent deposition of SAM molecules and perovskites by dissolving the former in the solution of the latter.[63] This approach simplifies the process, addresses the wettability issue of perovskites onto SAMs with low surface energies, and results in high device performance (24.5% efficiency and 1,200 h of $T_{>90}$ evaluated by the MPP tracking). Moreover, this method proves versatile across different SAM molecular systems together with perovskite compositions, solvents, and processing methods. Beyond the dominance of the aforementioned solution-based methods, vacuum-assisted physical vapor deposition has been developed to offer greater process flexibility.[64] This method tackles two major concerns: whether SAM molecules degrade at high processing temperatures and whether they are covalently adsorbed onto substrates. These concerns are mitigated by corroborating that the desired surface chemical properties are preserved. Notably, the surface energy of the Me-4PACz SAM is significantly altered, manifested by the water CA decreasing from 64.4 to 27.1°. Regardless of the deposition methods used, SAMs may form as multilayers, increasing their thickness. While rinsing after deposition could mitigate this issue, we hypothesize that thick SAMs could add resistivity during hole selection, potentially degrading device performance. However, a detailed understanding of this phenomenon has yet to be established. For instance, it remains uncertain whether thick SAMs−not prepared via codeposition but others−reduce their thickness after perovskite deposition through interactions with precursor solutions and antisolvents and/or with perovskite nuclei or crystals during annealing. In addition, the molecular orientation and number of layers in thick SAMs, both before and after perovskite deposition, and their impact on device performance remain unclear, warranting thorough examination in future studies.

Introducing Interlayers. *Interlayer Below SAM.* An interlayer between the substrate and SAM is added on the purpose of protecting the ITO surface from corrosion by acids, iodine, and other factors, minimizing the adverse effects of the ITO crystalline facets and surface roughness on SAM defects formation, mitigating the sensitivity of the UVO pretreatment to WF of ITO, and promoting a hydroxylated surface for SAM adsorption via strong chemical bonds. NiO_x is a favorable choice for an interlayer due to its properties as a p-type semiconductor that facilitates hole transport between the substrate and SAM while tackling the above issues. To this end, hydroxyl-rich NiO_x is coated onto ITO substrates by atomic layer deposition.[15] Prominently increased SAM molecule (MeO-2PACz) density and hence reduced batch-to-batch variations of devices are resultant outputs (see Figure 4d). NiO_x can also be processed in the form of nanoparticles by solution deposition. Incorporating hydrogen peroxide into the NiO_x nanoparticle solution can relax particle aggregation and enhance the transition of $Ni(OH)_2$ to NiOOH for conductivity and more surface hydroxyls for SAM adsorption.[65] Accordingly, a more homogeneous Me-4PACZ SAM is formed which is beneficial for the growth of perovskite over large areas.[65]

Interlayer above SAM. The insertion of an interlayer between the SAM and perovskite serves multiple purposes: promoting perovskite lamination, suppressing nonradiation recombination, improving interface passivation and dipole moment, and regulating perovskite crystallization. For example, methylenediamine makes the Me-4PACz SAM more wettable to the perovskite.[4] An ultrathin ionic layer of potassium fluoride (KF) between the 2PACz SAM and the perovskite can bolster the SAM dipole moment toward higher hole selectivity. This is driven by an ion-dipole interaction between F^- and 2PACz that outweighs intermolecular interaction.[66] Concurrently, interface defects are repaired by K^+ for halide vacancies and F^- for Pb^{2+} and organic ammoniums through hydrogen bonding. On top of the Me-4PACz SAM, Al_2O_3 nanoparticles are overlaid, which can increase roughness while maintain nearly unaltered ITO WF.[35] The pores between these nanoparticles act as pinning sites for the perovskite precursor solution, yielding complete coverage of perovskite.[35] The excellent perovskite coverage is attainable by overlaying PFN-Br (see Figure 4e), however, the Shockley-Read-Hall recombination is better suppressed by Al_2O_3 having an amphoteric nature. The challenge of inserting a low-conductive, ultrathin insulating interlayer is balancing between the V_{OC} and FF. A ∼ 100 nm thick layer of Al_2O_3 nanoplates with random nanoscale openings (reducing contact area by ∼ 25%) can circumvent this issue while leveraging the benefits of interlayers.[67] This configuration lowers surface recombination velocity from 64.2 to 9.2 cm s^{-1} on account of a lower trap

https://doi.org/10.1021/acsenergylett.4c03228
ACS Energy Lett. 2025, 10, 1292−1312

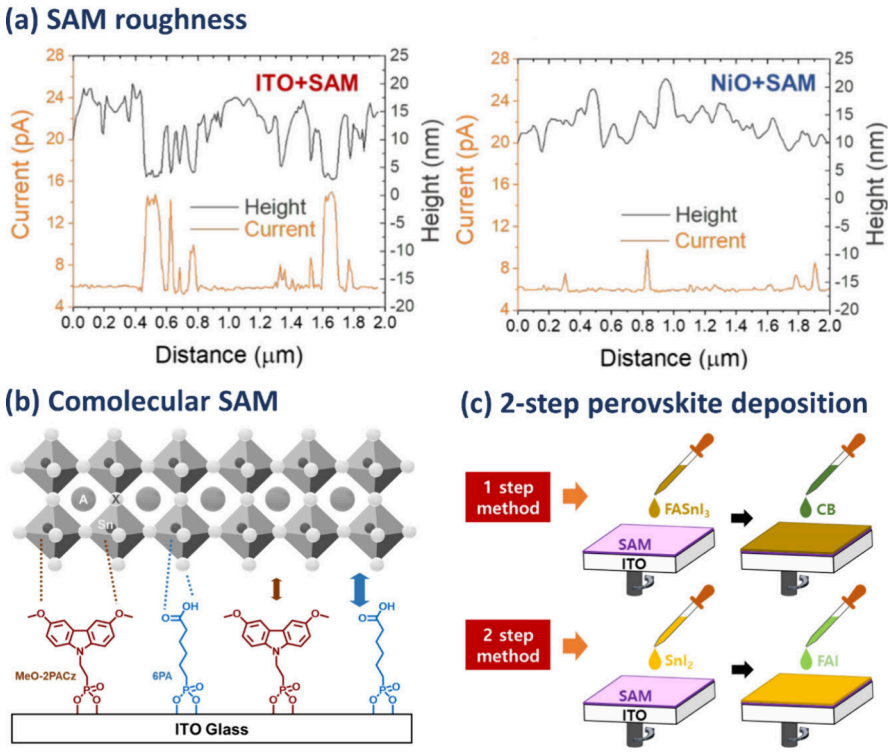

Figure 5. (a) The line profiles of ITO + MeO-2PACz and NiO + MeO-2PACz layers derived from the conducting atomic force microscope height and current maps.[15] Reproduced with permission from American Chemical Society, Copyright 2021. (b) Schematic illustration of the interaction between a Sn perovskite and different SAM molecules: MeO-2PACz and 6PA. In the perovskite crystal, A, X, and Sn stand for ammonium cations, halide anions, and divalent tin.[10] Reproduced with permission from American Chemical Society, Copyright 2024. (c) Schematic demonstration showing two different perovskite deposition methods atop the ITO/MeO-2PACz SAM. In the one-step deposition, $FASnI_3$ was directly spin-coated, during which an antisolvent chlorobenzene (CB) was injected. In the two-step deposition, the SnI_2 in DMSO and FAI in a cosolvent system were sequentially deposited using spin-coating to form $FASnI_3$.[16] Reproduced with permission from American Chemical Society, Copyright 2021.

density and extends the bulk recombination lifetime from 1.2 to 6.0 ms because of ameliorated perovskite crystallinity. As a result, the product of V_{OC} and FF reaches 87.9% of the SQ limit.

Perovskite Engineering. The polymer of β-poly(1,1-difluoroethylene) was used as an additive to tailor the perovskite deposited onto the MeO-2PACz SAM.[36] This polymer, possessing highly ordered dipolar structure, effectively interacts with the perovskite components by which void formation is suppressed and perovskite crystal grains are enlarged (see Figure 4f). In addition, it offers a strain-buffering and lattice stabilizing effects under thermal stress ranging from −60 to 80 °C. Meanwhile, one appealing recent development includes adopting a triple cosolvent system of DMF, DMSO, and *N*-methyl-2-pyrrolidone (NMP) to formulate the perovskite precursor solution for deposition atop the Me-4PACz SAM.[68] NMP − presenting a relatively nonpolar nature− facilitates binding of the perovskite solution to the SAM as evidenced by the DFT calculations and CA measurements. The facilitated binding leads to the formation of perovskite films with high coverage over device active areas ranging 0.16−1.08 cm^2.

Top surface passivation strategies for enhanced efficiency and stability have been reported. By applying oleylammonium iodide molecules, the Ruddlesden−Popper−phase 2D perovskite layers were formed to passivate the 3D perovskites in 2PACz SAM-based PSCs.[69] This approach allowed for high efficiency, accompanied by high stability under damp-heat test conditions (85 °C and 85% relative humidity). Meanwhile, piperazinium diiodide molecules are used as an additive, enabling passivation of deep-level defects, homogenization of potential distribution, and appropriate band bending on the top surface.[24] In Me-4PACz devices, a high PCE of 26.15% and decent MPP tracking stability (1,000 h of $T_{94.2}$) were achieved.[24] While passivator ligands are often electrically insulating and their dense packing perpendicular to the interface may limit FF of PSCs, 4-chlorobenzenesulfonate molecules that are prone to align in a planar orientation with dual binding-sites are developed to tackle this issue.[3] Their interaction with undercoordinated Pb^{2+} ions declines the surface defect density and minimizes the energetic mismatch between the perovskite and the ESL. Used in 2PACz/Me-4PACz co-SAM-based devices, the molecules contribute to a certified high efficiency of 26.15% and MPP tracking stability at 65 °C (T_{95} of 1,200 h).

Main Takeaway. Although the results of the aforementioned approaches vary from strategy to strategy, the principal goals of these approaches are to improve SAM quality in terms of packing density, orientation, dipole moment, stability, SAM interface properties, perovskite quality, or a combination thereof. While these approaches have driven recent impressive advancements in Pb (and Sn−Pb) PSCs and are still evolving, many of them merit adoption for Sn PSCs. On the other hand, Sn perovskites possess unique chemistry and crystallographic structure. With these two perspectives in mind, we will now

https://doi.org/10.1021/acsenergylett.4c03228
ACS Energy Lett. 2025, 10, 1292−1312

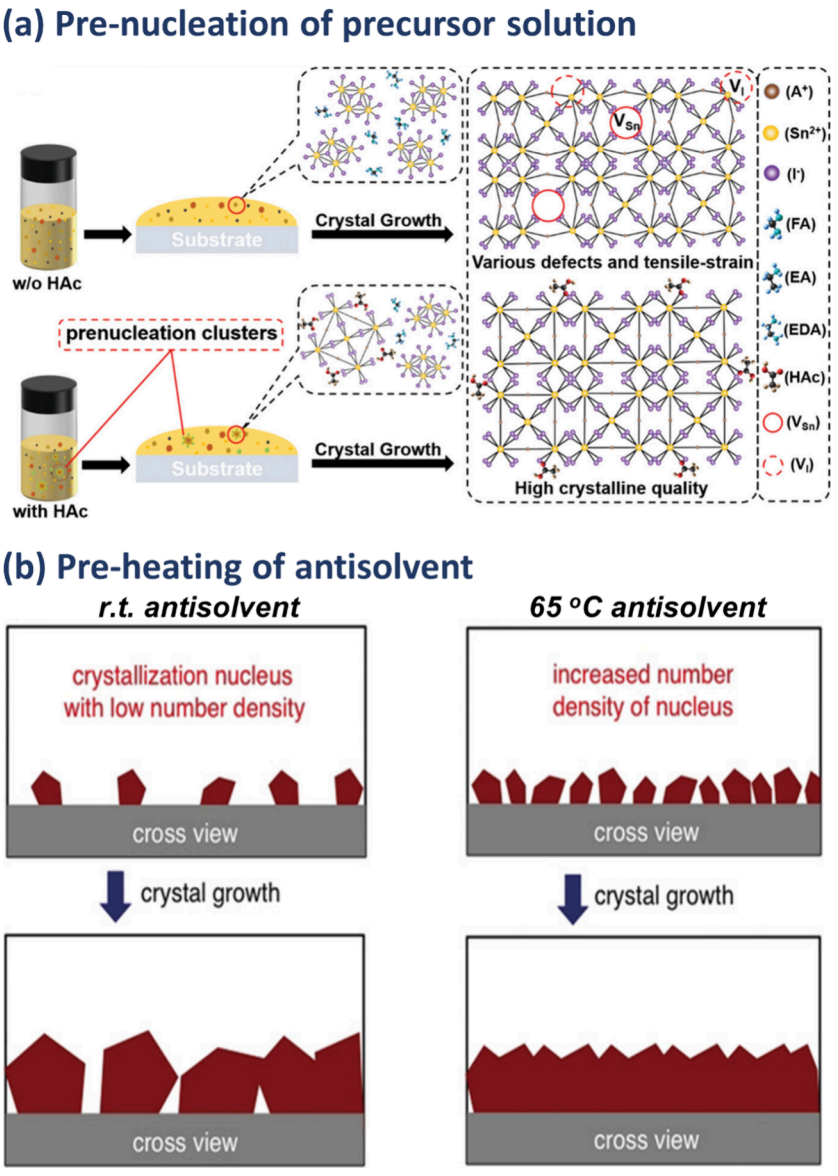

Figure 6. (a) Schematic illustration: the effect of acetic acid (HAc) on regulation of crystallization kinetics and improvement of crystalline quality.[80] Reproduced with permission from Wiley-VCH, Copyright 2021. (b) Illustration of $FA_{0.75}MA_{0.25}SnI_3$ film formation mechanism using r.t. antisolvent or antisolvent preheated to 65 °C.[82] Reproduced with permission from Wiley-VCH, Copyright 2018.

discuss what should be further developed for SAM HSL-based Sn PSCs, focusing on the following topical issues.

■ PERSPECTIVE ON PRINCIPAL ISSUES IN SN PSCS USING SAM HSLS

HSL Roughness. The present-day high-performance HSL for Sn PSCs is namely PEDOT:PSS.[13] It can show a very smooth surface with the root-mean-square roughness less than 1.5 nm on the ITO surface.[70] However, the SAM roughness tends to be higher, exemplified by over 2 nm for the MeO-2PACz SAM.[15] Even though the roughness discrepancy may slightly vary depending on the type of ITO glass, it mainly arises because the SAM forms with high conformality to the granular (i.e., relatively rough) ITO surface, in contrast to PEDOT:PSS. The addition of nanocrystalline NiO_x in thin films can partially flatten the rough ITO surface for SAMs to appreciable extent as Figure 5a shows. On a side note, NiO_x can homogenize the distribution of SAM molecules due to the increased content of hydroxyl groups compared to ITO.[14,15] We note that thick and porous NiO_x films, used in mesoscopic PSCs,[71] differ from the aforementioned thin NiO_x films. Oxygen surface etching can reduce the roughness to 1.35 nm.[30] The polymerized SAM molecule of poly(carbazole phosphonic acid) can smooth the surface.[57] We note that the high roughness could give rise to the creation of void defects at the SAM/perovskite interface. We envision that this issue would become more problematic for Sn perovskites, which crystallize rapidly. The outperformance of PEDOT:PSS/SAM and NiO_x/SAM HSLs over a SAM only HSLs in Sn PSCs might be explained by this. To corroborate this issue, a future investigation on the buried SAM interface by microscope imaging is required.

Lamination of Perovskite Films. The PEDOT:PSS HSL can exhibit a low CA of water (~10°) and a high surface energy (~73 mN/m).[10] Notably, the polar component of its surface energy is more than 4-fold greater than that of the MeO-2PACz SAM. It is worth remarking that the MeO-

https://doi.org/10.1021/acsenergylett.4c03228
ACS Energy Lett. 2025, 10, 1292−1312

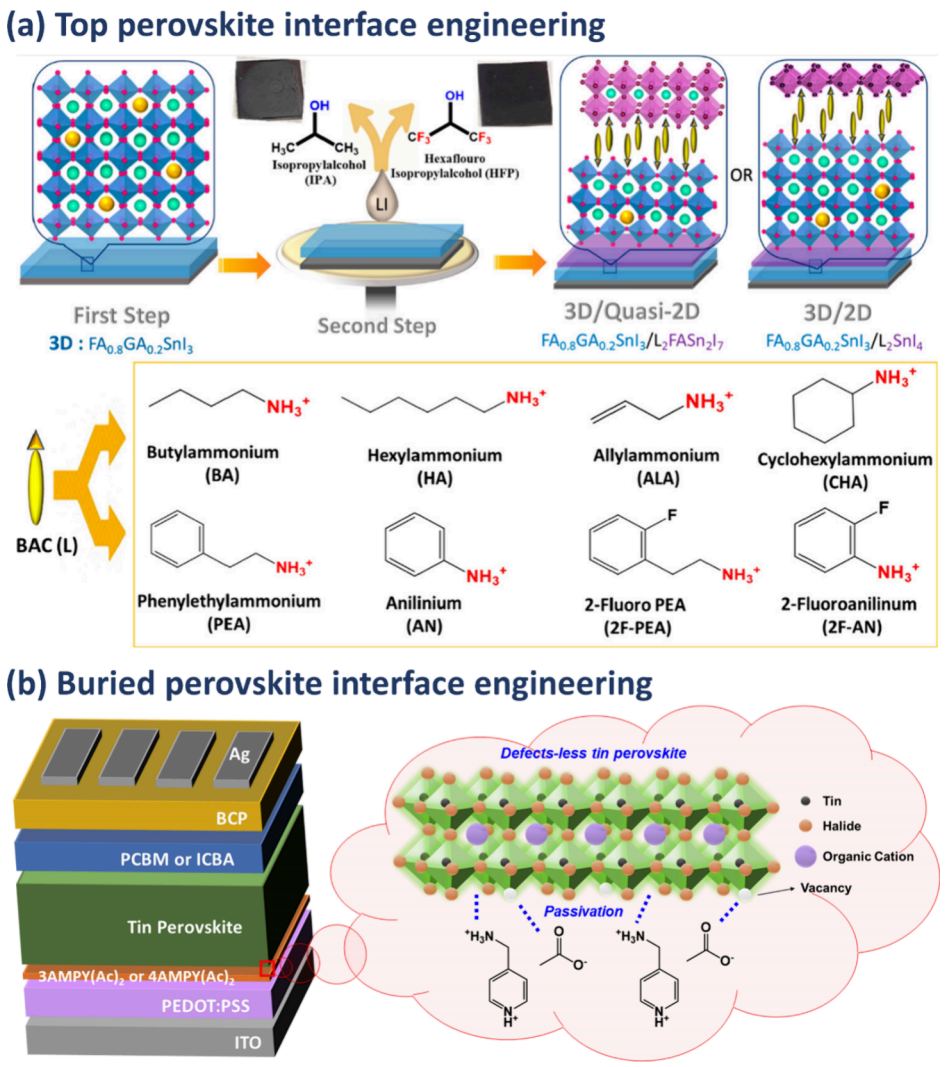

Figure 7. (a) Schematic representation of sequential deposition to grow a low-dimensional perovskite phase on the 3D layer ($FA_{0.8}GA_{0.2}SnI_3$, abbreviated as E1G20) in the second step using one of eight bulky ammonium cations (BAC, represented by L) as indicated. The top photographs show the effect of solvents (left, IPA; right, HFP) applied in the second step to dissolve the LI salts.[87] Reproduced with permission from American Chemical Society, Copyright 2021. (b) Schematic illustrations of post-treatment with 4AMPY(Ac)$_2$ onto the PEDOT:PSS HTL in a device with 4AMPY(Ac)$_2$.[70] Reproduced with permission from American Chemical Society, Copyright 2023.

2PACz SAM presents relatively small CAs relative to others. The PSS enriched surface in PEDOT:PSS and the methoxy dangling moiety in MeO-2PACz elevate their polarity to be more interactive with perovskites by hydrogen and coordination bonds, respectively. Specifically for PEDOT:PSS, we thus posit that owing to its large polar component, coupled with the smooth surface, Sn perovskites are nearly seamlessly laminated onto PEDOT:PSS. Future efforts to enhance the polar component toward a more wettable surface will be essential for applications to SAM HSL-based Sn PSCs. For example, introducing interlayers above SAMs such as Al_2O_3, PFN-Br, and KF could find suitability for Sn PSCs as NiO_x does, which is so far not being studied yet (see Supporting Information). In an alternative way, comolecular SAMs with a myriad of material combinations and ratios warrant extensive exploration, as demonstrated by the MeO-2PACz and 6PA SAMs for Sn PSCs (Figure 5b). As discussed earlier, a superwettable HSL surface by designing SAM functional groups is desirable to the extent that gaseous H_2O and O_2 − prevailing in surroundings− being capable of degrading tin perovskites and their interfaces are not invasive. Vacuum-aided SAM deposition, which can raise surface energy of Me-4PACz remarkably to improve coverage of the Pb perovskite films,[64] is available and should be further developed for Sn PSCs.

The lamination partially hinges on the perovskite deposition method. Therefore, in parallel with optimizing SAM surface properties, developing suitable perovskite deposition methods is required for perovskite lamination. Straightforwardly, depositing the SAM together with the perovskite (namely, the codeposition method) could potentially resolve the lamination issue, thus finding suitability for Sn PSCs. In cases where a one-step antisolvent-reliant deposition is used, both the precursor solution and antisolvent should be optimized in terms of volume and type due to the sensitivity of perovskite film thickness to the SAM.[10] Switching a one-step deposition method to another would offer a technical solution. For example, the two-step method of sequentially depositing the SnI_2 and FAI precursor solutions−described in Figure 5c− can be effective for perovskite lamination likely because of the low CAs (below ~ 20°) of the SnI_2 solution (see Supporting

https://doi.org/10.1021/acsenergylett.4c03228
ACS Energy Lett. 2025, 10, 1292−1312

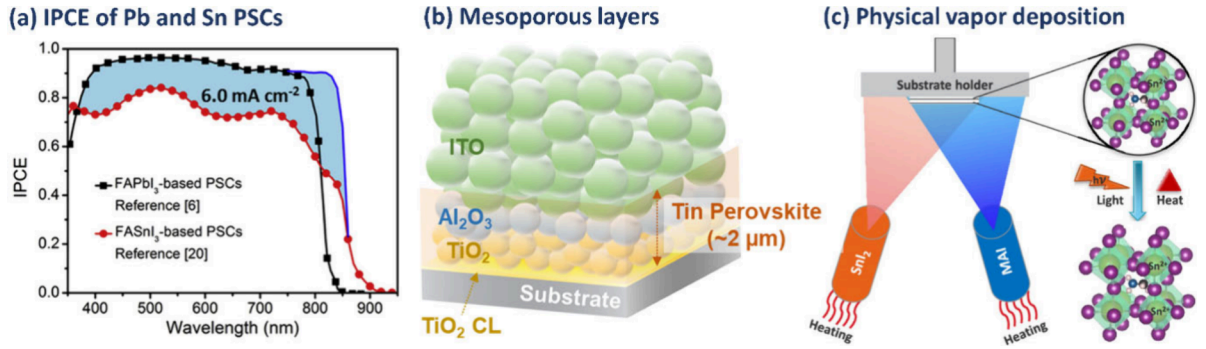

Figure 8. (a) Incident photon-to-current conversion efficiency (IPCE) spectra of the best certified lead and tin PSCs. The integrated J_{SC} is calculated to be 26.1 and 22.4 mA cm^{-2} for lead and tin PSCs, respectively.[97] Reproduced with permission from Elsevier, Copyright 2021. (b) Illustration of the mesoporous device incorporating thick tin perovskite.[96] Reproduced with permission from Elsevier, Copyright 2023. (c) Illustration of coevaporation of CH_3NH_3I and SnI_2 to obtain absorbers with Sn being only in the preferred oxidation state [+2].[98] The absorber films show very good stability under heat and light. Reproduced with permission from American Chemical Society, Copyright 2022.

Information), the long contact time of the SnI_2 layer on the SAM (from its spin-coating to FAI layer deposition), and the relatively slow crystallization process (usually over 10 s, compared to just a few seconds in one-step deposition).[16] Beyond the solution-processing, the vapor- or vacuum-assisted deposition method to enable the formation of Sn perovskite films conformal to SAMs should be free of delamination issues to encourage future research endeavors.

Perovskite Crystallization. Regulating the crystallization kinetics of Sn perovskites in a judicious manner could help improve crystal quality (e.g., crystallinity, crystal orientation) as well as lamination. The topic of improving crystallization has been dealt with several review papers.[72,73] However, it is important to remark that crystallization should be further developed on SAM HSLs, potentially using refined or novel materials and methods. In addition, fundamental parameters for perovskite deposition including precursor solution volume and loading time, as well as the type, volume, and injection method of the antisolvent can play a pivotal role in optimizing the process.[10]

It has been revealed that the strong Lewis acidity of Sn^{2+} and relatively low solubility of SnI_2 to instantly react with organic or inorganic halides drive rapid crystallization of Sn perovskites compared to their lead counterparts. This poses a great challenge toward attaining perovskite crystals possessing all the desired properties simultaneously such as high crystallinity, preferred orientation, large grain size, and pinhole-free films not only on PEDOT:PSS but also on SAMs. For example, the preferred orientation is better realized with the MeO-2PACz/6PA SAM than with PEDOT:PSS, but at the expense of overall crystallinity.[10] In this regard, it is urged to revisit the approaches developed to date for SAM-free HSLs (mostly PEDOT:PSS) for a strengthened perovskite quality. In particular, incorporating additives and cations into perovskite precursor solutions is a good starting point, with examples including thioureas,[12,74] pyridines,[25,75] n-propylammonium iodide,[12] ethylenediammonium diiodide,[76] and 2-phenylethylammonium iodide.[77] While rapid crystallization gives rise to fast nucleation and crystal growth, incomplete nucleation (i.e., low nuclei density) − likely resulting in poor morphology and unreacted perovskite precursors−is thought to be prevailing in Sn perovskites. Nuclei would be more sparse on SAM HSLs due to the smaller surface energies than PEDOT:PSS.[78] To densify nuclei, approaches such as poly(vinyl alcohol) or acetic acid as an additive,[79,80] heating the precursor solution or antisolvent,[81,82] and adopting acetic acid antisolvent[83] as an antisolvent have been attempted, whose representative examples are illustrated in Figure 6. While heterogeneous nucleation is thermodynamically favorable, its Gibbs free energy (i.e., the activation energy) decreases as the perovskite solution exhibits greater wettability on the HSL surface. This implies that increasing the surface energy of SAM HSLs through their molecular design with various functional groups (e.g., hydroxyl, carboxyl, or amino groups) could promote the densification of perovskite nuclei. However, this seems to contradict the SAM interface with Pb perovskite, as it reflects the rapid crystallization of Sn perovskite. Meanwhile, if we assume that the crystallization occurs downward from the perovskite/air interface,[84] residual solvents may linger and be trapped at the buried SAM HSL interface since the low volatile solvents including DMSO or DMF/DMSO and the low annealing temperatures (usually, below 100°) are applied for Sn perovskites. The residual solvents would ultimately create voids or pinhole defects.[85] While this issue requires further research, declining the proportion of DMSO or replacing it with volatile solvents will likely be necessary.

Top and Buried Perovskite Interface Engineering. On the top surface of Sn perovskite films, the unique defects of Sn(IV) with propensity to create tin vacancies become enriched and some of these defects contribute to the formation of SnO_2.[86] This unregulated surface significantly hampers electron extraction, thereby negating the effect of SAM HSLs and diminishing the device performance. On this point, the top interface engineering is pivotal. One example is shown in Figure 7a. Upgrading the perovskite top surface using a 2D layer with anilinium iodide,[87] passivation layers with 6-maleimidohexanehydrazide trifluoroacetate, acetylacetone and ethylenediamine,[88,89] and a dipole layer with 4-fluorophenethylamine hydrobromide,[12] and/or replacing the widely used ESL of C60 (buckminsterfullerene) with ICBA[90] or the diethylmalonate-C60 bisadduct[91] should be explored. Specifically, C60 or its analogs would possess non-negligible in-gap defect states that facilitate recombination. Indeed, it has been verified that the ICBA ESL significantly improves the V_{OC} of SAM-based Sn PSCs as presented in Table 1.

SAMs demonstrate the capability to reduce interfacial defects more effectively than conventional HSLs, such as

https://doi.org/10.1021/acsenergylett.4c03228
ACS Energy Lett. 2025, 10, 1292−1312

PEDOT:PSS.[92] Though, the buried interface engineering of Sn perovskite films is encouraged in light of further reducing the defects and passivating uncovered substrate regions with SAM molecules. In this regard, the buried perovskite interface engineering that was applied to PEDOT:PSS[70,93,94] will be attractive. One such example of PEDOT:PSS is presented in Figure 7b. Nonetheless, it is important to note that buried interface modification on SAMs must be handled with caution, as it could be compromised by the deposition of the subsequent perovskite layer.

By leveraging the aforementioned remedies for perovskite lamination, crystallization, and interface engineering, SAM-based Sn PSCs can outpace PEDOT:PSS devices and cross the 50% threshold in PCE (Figure 3a). With strong optimizm for further advancements toward the 75% threshold and beyond, we delve into additional but still critical issues in the following.

Increasing Perovskite Film Thickness. Sn perovskite films (thickness: ∼ 200−300 nm) are thinner than lead perovskite films (> ∼ 500 nm) for solar cell applications, despite their comparable light extinction coefficients. The thinner films lead to an overall reduction in light collection across the entire absorption range (Figure 8a), resulting in a substantial J_{SC} deficit. They are formed at relatively low concentrations (< 1.0 M) of the perovskite precursor solution. One report assesses the thickness−PCE relationship in the range of 150 to 300 nm, disclosing that a 200 nm Sn perovskite film led to the best performance.[95] The key photovoltaic parameter to determine this thickness is apparently the J_{SC}. In principle, J_{SC} is influenced by both light and charge collection efficiencies, so increasing the film thickness induces their interplay to account for the 200 nm thickness might limit the effective charge carrier diffusion length for the tested perovskite films. In contrast, in triple mesoscopic devices, perovskite film thickness is adjustable over a wider range (up to several micrometers) by the predetermined structure of mesoporous layers (Figure 8b) and thick Sn perovskite films (∼ 2 μm) can achieve high J_{SC} (over 27 mA cm^{-2}).[96] This indicates that the effective charge carrier diffusion length remains unclear for Sn perovskite films and may be technically extendable. To enable thicker Sn perovskite films and, consequently, higher J_{SC}, efforts should be directed toward higher concentrations (≥ 1.0 M) of the perovskite precursor solution and/or taking advantage of the mesoporous layers. On the other hand, perovskite deposition methods, such as vapor or vacuum-aided deposition, would need to be advanced; one example on vapor deposition is presented in Figure 8c. Regardless of the efforts made, it is crucial to control perovskite crystallinity, bulk defects, and interfacial defects−particularly tin vacancy defects for p-doping, which would shorten the diffusion length of electrons−while ensuring seamless integration of perovskite films onto high-performance SAM HSLs.

Defect Control. In lead perovskite, point defects such as vacancy, interstitial, and antisite defects are likely present both within the interior and on the exterior of its crystals. Also, these defects are likely embedded in the tin perovskite crystals. However, conduction band and valence band edges are overall shallower with tin perovskite compared to lead perovskite with influence on energy levels of traps formed by the defects. According to the DFT calculations,[99] in tin perovskite, acceptor-type defects like iodide interstitial (I_i) and tin vacancy (V_{Sn}) defects are shallower, while donor-type defects like iodide vacancy (V_I) and tin interstitial (Sn_i) defects are deeper, relative to lead perovskite. Notably, deep-level traps serve as the primary source of charge trapping and give rise to nonradiative recombination losses.

Technically, the point defects of prime concern in lead perovskites are driven by migration of halide ions. In contrast, the major defects are formed in the tin perovskite by easy oxidation of tin. In specific, the redox potential of Sn(II)/Sn(IV) (+ 0.15 V vs SHE) is significantly lower than that of Pb(II)/Pb(IV) (+ 1.67 V vs SHE), concomitantly modulating defect activity differently between tin and lead perovskites and influencing their electronic features. The lower redox potential of Sn makes oxidation easier. The oxidation (Sn(II) to Sn(IV)) dislodges tin atoms from the perovskite lattice to form SnO_2 upon contact with oxygen, concurrent with creating vacancy defects. As a result, tin perovskites tend to be highly p-doped by the presence of tin vacancy defects. In contrast, lead perovskites have much greater resistance to oxidation, exhibiting nearly intrinsic character. In this regard, the primary approach should focus on suppressing the oxidation for tin perovskite, whereas for lead perovskite controlling ion migration is key. This distinction should be considered when designing the SAM/perovskite interface for Sn PSCs.

Attenuating tin vacancy defects can be demonstrated by suppressing Sn(IV) formation in precursor solutions, perovskite films, and devices. The detailed tin oxidation mechanism and mitigation methods are delineated from this perspective in several review papers.[100−103] Here, we specifically focus on the SAM/perovskite interface. It is recommended that the surface of SAM HSLs should be tailored with functional groups to prevent Sn perovskites from Sn(II) oxidation. If functional groups act as Lewis bases, such as groups of methoxy, sulfur, amine, cyano, and hydrazine, they can effectively stabilize undercoordinated Sn(II). Also, ammonium halide- or pseudohalide-terminated SAM molecules could stabilize undercoordinated Sn(II). We note that attention should be given to the presence of Sn(IV) in FTO and ITO substrates that could emerge as SAM/perovskite interface, which can be analyzed by photoelectron spectroscopy (the analysis depth: ∼ 1 to 10 nm).

Meanwhile, device encapsulation to further suppress the Sn(IV) formation is encouraged. Interestingly, hydrophobic SAMs fabricated using fluorinated molecules[104] were used to passivate Sn perovskite films and top metals like Ag likely with good conformality. Especially, the metal passivation, which directly targets the surface, differs from traditional encapsulation methods using a sealant and supporting substrate without direct contact. This approach is likely more effective in protecting tin perovskites from invasive harmful species such as gaseous H_2O and O_2.

Once tin vacancy defects (V_{Sn}) are controllable, other types of defects−such as vacancies (e.g., V_I and V_{FA}), interstitials (e.g., FA_i, Sn_i, and I_i), and antisite substitutions (e.g., FA_{Sn}, Sn_{FA}, FA_I, Sn_I, I_{FA}, and I_{Sn}) where FA stands for the formamidinium−are apt to be outstanding in bulk and interfaces of Sn perovskite films.[86] Interfacial defects are generally regarded to be more abundant than bulk defects. The implication of this is that the defect-lean interfaces of SAM HSLs will be crucial for upgrading the Sn PSCs to levels comparable to and exceeding those of Pb PSCs. This underscores the need for new research advances in the key strategies articulated here.

Energy Level Alignment. The hole transfer arguably takes place from the perovskite VBM to the SAM HOMO and ITO

https://doi.org/10.1021/acsenergylett.4c03228
ACS Energy Lett. 2025, 10, 1292−1312

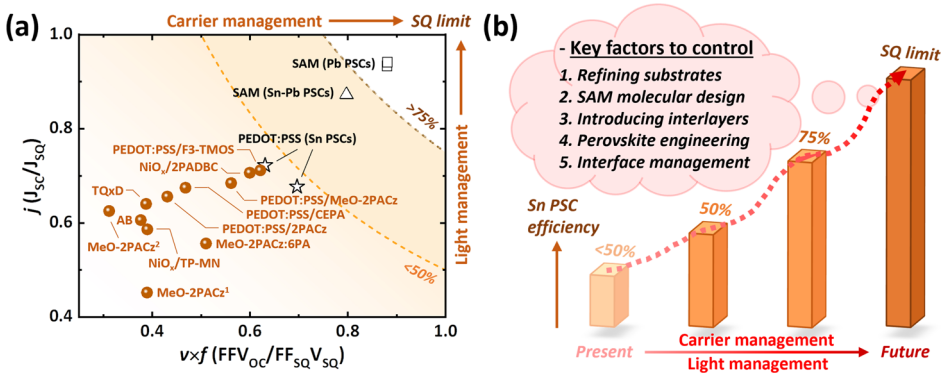

Figure 9. (a) The current ratio (j) versus the product of voltage and fill factor ratios ($v \times f$) is plotted for SAM HSLs-based Sn PSCs, using the data from Figures 2b–d. For comparison, the high-efficiency Pb and Sn–Pb devices using SAM HSLs as well as Sn PSCs with a PEDOT:PSS HSL are included. (b) The future research direction for SAM-based Sn PSCs is illustrated to surmount the hurdles (the 50% and 75% limits), focusing on carrier management and light management, with key controlling factors proposed.

WF. The transfer from the SAM to ITO would involve two different mechanisms: tunneling and injection. The non-conjugated SAM like MeO-2PACz could transfer holes by tunneling where the spacer breaks conjugation and its length alters tunneling efficiency. On the contrary, the conjugated SAM like TQxD could transfer holes by injection. Though, energy alignment at the SAM interface would affect hole transfer irrespective of the transfer mechanism.

The Sn perovskites in three-dimensions present VBM energy levels of −4.9–5.2 eV that are shallower than lead analogs due to the uplifted Sn 5s orbital level. Therefore, the energy alignment of existing HSLs, likely customized for Pb or Sn–Pb perovskites, with Sn perovskites would not be ideal; we note that the HOMO energy levels of the TQxD and TP-MN SAMs developed for Sn PSCs are shallow.[14,17] The SAM dipole moment can alter the ITO WF and SAM HOMO energy levels, as mentioned earlier. The ITO WF is adjustable by a net change in three contributions, the possible geometry relaxation of the surface, the molecular dipole moment normal to the surface, and the interfacial dipole.[59,105] The latter two can be major contributors and then the following equation can be used to calculate the WF change:

$$\Delta\phi = -N\left[\frac{\mu_{z,SAM}}{\varepsilon_0\kappa_{SAM}} + \frac{\mu_{ITO-SAM}}{\varepsilon_0\kappa_{ITO-SAM}}\right] \quad (2)$$

where N is the SAM coverage, $\mu_{z,SAM}$ is the dipole moment along the z-axis (normal to the surface), ε_0 is the vacuum permittivity, κ_{SAM} is the effective dielectric constant, and $\mu_{ITO-SAM}/(\varepsilon_0\kappa_{ITO-SAM})$ is the term associated with the interfacial dipole. The ITO WF is approximately 4.7 eV but can be adjusted by SAMs as much as ca. 1.5 eV. Meanwhile, the HOMO energy level tends to conform to the trend of WF changes.[29] The WF and HOMO energy level data of SAM HSLs on Sn PSCs are summarized in Table 1 and the Supporting Information. A more extensive library on PSCs can be found in literature.[29,92]

Tailoring SAM molecules, substrates, or their interfaces to maintain the appropriate energetic properties is encouraged for future research. More straightforwardly, one can take advantage of the comolecular SAM concept to systematically adjust the energetic properties, making them well-suited for tin perovskite. For example, MeO-2PACz can be combined with various other SAMs available in the library to achieve the desired outcomes.

Comparative Study. Cross-fertilization by comparative studies on HSL types (e.g., PEDOT:PSS vs. SAMs), perovskite types (e.g., Sn perovskite vs. Sn–Pb perovskite vs. Pb perovskite), and perovskite deposition methods (e.g., one-step vs. two-step) offers a powerful avenue for advancing SAM-based Sn PSCs. A widely used study is the comparison of photovoltaic parameters as we did in Figure 3. Moving forward, we further explore comparative studies by plotting Figure 9a using the data points from Figure 3, in light of two characteristic parameters, light management ($j = J_{SC}/J_{SQ}$) and carrier management ($v \times f = (V_{OC}/V_{SQ}) \times (FF/FF_{SQ})$), where J_{SQ}, V_{SQ}, and FF_{SQ} stand for the J_{SC}, V_{OC}, and FF at the SQ limit;[106] we note that in Figure 9a one can compare each device irrespective of perovskite bandgap, unlike in Figure 3. Light management relates to the degree of light coupling, absorption, and trapping in the perovskite layer and carrier collection efficiency. Carrier management reflects the extent of charge carrier recombination in the perovskite bulk and at the interface, along with the resistive losses and other nonidealities. As seen in Figure 9a, Sn PSCs perform below 50% of the S–Q limit and lag significantly behind Sn–Pb and Pb PSCs in both carrier management and light management. In common, all types of PSCs suffer from relatively poor carrier management, to varying degrees. All in all, in Sn PSCs, PEDOT:PSS/SAM and NiO_x/SAM HSLs provide better light management and carrier management compared to SAM alone. The previously mentioned Sn perovskite thickness and crystal quality are considered as poor light management (< 0.72 of j) and carrier management (< 0.63 of $v \times f$). In Figure 9b, we summarize five key factors to deal with to attain desired light management (> 0.9 of j) and carrier management (> 0.9 of $v \times f$) including 1) refining substrate, 2) SAM molecular design, 3) introducing interlayers, 4) perovskite engineering, and 5) interface management, by which SAM-based Sn PSCs can surpass 50% and 75% of the SQ limit, ultimately approaching 100%. On a further note, it is formidable to accurately predict how each key factor impacts light management and carrier management, respectively, at this time. However, it should be emphasized that these five key factors are fundamental to addressing the principal issues discussed in this Section.

Meanwhile, future research should focus on comparative studies of light and carrier management using a broader range of SAM materials. Besides, more specific characteristic parameters should be introduced to deepen the understanding of the fundamentals and seek further solutions, exemplified by

https://doi.org/10.1021/acsenergylett.4c03228
ACS Energy Lett. 2025, 10, 1292–1312

hole transfer and recombination rates at the SAM interface. Measurements of transient surface photovoltage, photoluminescence decay profiles, femtosecond transient absorption, and others are available for this purpose. One should consider that this SAM interface would entail excluding the effects of perovskite crystal quality on hole transfer and recombination kinetics.

Up-Scaling Efforts. Following progress toward a commercial level (competitive with or surpassing Pb PSCs), Sn PSC fabrication is transitioning from laboratory-scale to industrial-scale production. This transition requires additional processes for re-engineering materials and methods, as well as implementing sophisticated steps such as laser scribing, alignment, and interconnection, among others. Some of these processes have to be carried out under ambient air conditions, which necessitates the high stability of Sn PSCs. Therefore, efforts to enhance the stability of tin perovskites and their interfaces are critical for commercialization. We further note that these efforts could also promote high reproducibility.

Inspiringly, a recent report reveals that one path to achieving high device stability involves replacing a PEDOT:PSS HSL with a more robust HSL.[107] During laser scribing, the deposited layers of HSL/tin perovskite/ESL/metal are partly etched and exposed to ambient air. In this process, PEDOT:PSS tends to absorb moisture, leading to degradation of both itself and its interfaces, resulting in a mere 1% device efficiency. In contrast, the robust HSL composed of PEDOT/Al_2O_3 avoids this issue, enabling a higher efficiency of 5.7%. We anticipate that SAM, which is relatively less hydroscopic—could replace PEDOT:PSS to further stabilize large-scale devices for higher efficiency and stability.

Beyond hygroscopicity, other factors, including the molecular structural stability of SAMs, should be taken into account to achieve high stability. To date, research on this topic, particularly at the device level, remains limited. To address this gap, the high tunability of the SAM molecules could be leveraged. One potential approach involves hypothesizing that conjugated spacer groups may offer greater stability compared to others. Validating this hypothesis will require post-mortem device analysis.

CONCLUSIONS

Sn perovskite solar cells using hole-selective self-assembled monolayers are highly promising on account of their high efficiency potential and low toxicity. However, their performance is inferior to that of lead-based counterparts due to poor light management and carrier management together with low stability. The issues to deal with are multifaceted, spanning substrates, SAMs, perovskites, and interfaces thereof. They include, specifically, SAM roughness and energy level and perovskite lamination, thickness, and crystal quality as well as interface passivation engineering. Implementing methodical approaches across diverse materials and processing methods is essential to tackle these issues. Comparative studies across distinct SAM and perovskite types can offer complementary insights. The successful implementation of these approaches will promise that Sn perovskite solar cells will close the gap with and eventually surpass competitors in the pursuit of sustainable single-junction and likely tandem photovoltaics. This progress could facilitate the development of Sn perovskite and SAM-based applications in energy and electronics, including light-emitting diodes, photodetectors, and transistors, among others, toward outperformance and upscaling.

ASSOCIATED CONTENT

Supporting Information

The Supporting Information is available free of charge at https://pubs.acs.org/doi/10.1021/acsenergylett.4c03228.

Summary of key properties of SAM-based Sn PSCs (XLSX)

AUTHOR INFORMATION

Corresponding Authors

Donghoon Song − *School of Materials Science and Engineering, Georgia Institute of Technology, Atlanta, Georgia 30332, United States;* orcid.org/0000-0003-0914-1507; Email: dsong93@gatech.edu

Eric Wei-Guang Diau − *Department of Applied Chemistry and Institute of Molecular Science, National Yang Ming Chiao Tung University, Hsinchu 300093, Taiwan; Center for Emergent Functional Matter Science, National Yang Ming Chiao Tung University, Hsinchu 300093, Taiwan;* orcid.org/0000-0001-6113-5679; Email: diau@nycu.edu.tw

Juan-Pablo Correa-Baena − *School of Materials Science and Engineering, Georgia Institute of Technology, Atlanta, Georgia 30332, United States; School of Chemistry and Biochemistry, Georgia Institute of Technology, Atlanta, Georgia 30332, United States;* orcid.org/0000-0002-3860-1149; Email: jpcorrea@gatech.edu

Authors

Seung Wook Shin − *Future Agricultural Research Division, Rural Research Institute, Korea Rural Community Corporation, Ansan 15634, South Korea;* orcid.org/0000-0002-3396-2535

Hui-Ping Wu − *Department of Applied Chemistry and Institute of Molecular Science, National Yang Ming Chiao Tung University, Hsinchu 300093, Taiwan*

Complete contact information is available at: https://pubs.acs.org/10.1021/acsenergylett.4c03228

Notes

The authors declare no competing financial interest.

Biographies

Donghoon Song is a researcher at the Georgia Institute of Technology in the USA, specializing in perovskite solar cells. His specific interests in perovskite solar cells encompass tin perovskites, interface materials and engineering, and the fundamental relationships between property, structure, and performance.

Seung Wook Shin is a senior research professor at the Rural Research Institute, Korea Rural Community Corporation. His work focuses on the synthesis and characterization of inorganic energy conversion materials and their applications, including thin-film solar cells and photoelectrochemical water-splitting devices.

Hui-Ping Wu received her Ph.D. degree in Applied Chemistry from National Yang Ming Chiao Tung University, Taiwan, in 2014. She has subsequently worked as a postdoctoral researcher at the same institute. Her research efforts have been focused on dye-sensitized solar cells, perovskite solar cells, and electrochemical synthesis and measurements.

Eric Wei-Guang Diau is now a chair professor at the Department of Applied Chemistry and the Institute of Molecular Science at National Yang Ming Chiao Tung University. His research interests include dye-

https://doi.org/10.1021/acsenergylett.4c03228
ACS Energy Lett. 2025, 10, 1292−1312

sensitized and perovskite solar cells, photocatalysis and femtochemistry. https://diau08.lab.nycu.edu.tw/en/

Juan-Pablo Correa-Baena is an Associate Professor and the Goizueta Junior Faculty Chair in the School of Materials Science and Engineering and the School of Chemistry and Biochemistry at Georgia Institute of Technology. He is interested in developing deposition techniques, exploiting advanced characterization methods, and understanding fundamentals for emerging optoelectronic materials. https://baena.gatech.edu/

■ ACKNOWLEDGMENTS

JPCB and DS acknowledge support from the Georgia Institute of Technology. EWGD and HPW gratefully acknowledge the support by the National Science and Technology Council (NSTC), Taiwan (grant No. NSTC 113-2639-M-A49-001-ASP), the Center for Emergent Functional Matter Science of National Yang-Ming Chiao-Tung University (NYCU) from the Featured Areas Research Center Program within the framework of the Higher Education Sprout Project by the Ministry of Education (MOE) in Taiwan.

■ REFERENCES

(1) Li, M.; Liu, M.; Qi, F.; Lin, F. R.; Jen, A. K.-Y. Self-Assembled Monolayers for Interfacial Engineering in Solution-Processed Thin-Film Electronic Devices: Design, Fabrication, and Applications. *Chem. Rev.* **2024**, *124* (5), 2138−2204.

(2) Love, J. C.; Estroff, L. A.; Kriebel, J. K.; Nuzzo, R. G.; Whitesides, G. M. Self-Assembled Monolayers of Thiolates on Metals as a Form of Nanotechnology. *Chem. Rev.* **2005**, *105* (4), 1103−1170.

(3) Chen, H.; Liu, C.; Xu, J.; Maxwell, A.; Zhou, W.; Yang, Y.; Zhou, Q.; Bati, A. S. R.; Wan, H.; Wang, Z.; Zeng, L.; Wang, J.; Serles, P.; Liu, Y.; Teale, S.; Liu, Y.; Saidaminov, M. I.; Li, M.; Rolston, N.; Hoogland, S.; Filleter, T.; Kanatzidis, M. G.; Chen, B.; Ning, Z.; Sargent, E. H. Improved Charge Extraction in Inverted Perovskite Solar Cells with Dual-Site-Binding Ligands. *Science* **2024**, *384* (6692), 189−193.

(4) Ugur, E.; Said, A. A.; Dally, P.; Zhang, S.; Petoukhoff, C. E.; Rosas-Villalva, D.; Zhumagali, S.; Yildirim, B. K.; Razzaq, A.; Sarwade, S.; Yazmaciyan, A.; Baran, D.; Laquai, F.; Deger, C.; Yavuz, I.; Allen, T. G.; Aydin, E.; De Wolf, S. Enhanced Cation Interaction in Perovskites for Efficient Tandem Solar Cells with Silicon. *Science* **2024**, *385* (6708), 533−538.

(5) Pitaro, M.; Tekelenburg, E. K.; Shao, S.; Loi, M. A. Tin Halide Perovskites: From Fundamental Properties to Solar Cells. *Adv. Mater.* **2022**, *34* (1), 2105844.

(6) Chen, M.; Kapil, G.; Wang, L.; Razey Sahamir, S.; Baranwal, A. K.; Nishimura, K.; Sanehira, Y.; Zhang, Z.; Akmal Kamarudin, M.; Shen, Q.; Hayase, S. High Performance Wide Bandgap Lead-Free Perovskite Solar Cells by Monolayer Engineering. *Chem. Eng. J.* **2022**, *436*, 135196.

(7) Cho, S.; Pandey, P.; Yoon, S.; Ryu, J.; Lee, D.-G.; Shen, Q.; Hayase, S.; Song, H.; Choi, H.; Ahn, H.; Oh, C.-M.; Hwang, I.-W.; Cho, J. S.; Kang, D.-W. Anchoring Self-Assembled Monolayer at Perovskite/Hole Collector Interface for Wide Bandgap Sn-Based Solar Cells with a Record Efficiency over 12%. *Surf. Interfaces* **2023**, *42*, 103478.

(8) Kapil, G.; Bessho, T.; Sanehira, Y.; Sahamir, S. R.; Chen, M.; Baranwal, A. K.; Liu, D.; Sono, Y.; Hirotani, D.; Nomura, D.; Nishimura, K.; Kamarudin, M. A.; Shen, Q.; Segawa, H.; Hayase, S. Tin-Lead Perovskite Solar Cells Fabricated on Hole Selective Monolayers. *ACS Energy Lett.* **2022**, *7* (3), 966−974.

(9) Zhang, Z.; Zhu, R.; Tang, Y.; Su, Z.; Hu, S.; Zhang, X.; Zhang, J.; Zhao, J.; Xue, Y.; Gao, X.; Li, G.; Pascual, J.; Abate, A.; Li, M. Anchoring Charge Selective Self-Assembled Monolayers for Tin-Lead Perovskite Solar Cells. *Adv. Mater.* **2024**, *36* (18), 2312264.

(10) Song, D.; Ramakrishnan, S.; Zhang, Y.; Yu, Q. Mixed Self-Assembled Monolayers for High-Photovoltage Tin Perovskite Solar Cells. *ACS Energy Lett.* **2024**, *9* (4), 1466−1472.

(11) Teng, T.-Y.; Su, Z.-H.; Hu, F.; Chen, C.-H.; Chen, J.; Wang, K.-L.; Xue, D.; Gao, X.-Y.; Wang, Z.-K. Electronically Manipulated Molecular Strategy Enabling Highly Efficient Tin Perovskite Photovoltaics. *Angew. Chem., Int. Ed.* **2024**, *63* (7), No. e202318133.

(12) Shi, Y.; Zhu, Z.; Miao, D.; Ding, Y.; Mi, Q. Interfacial Dipoles Boost Open-Circuit Voltage of Tin Halide Perovskite Solar Cells. *ACS Energy Lett.* **2024**, *9* (4), 1895−1897.

(13) Song, D.; Ramakrishnan, S.; Xu, Y.; Yu, Q. Designing Effective Hole Transport Layers in Tin Perovskite Solar Cells. *ACS Energy Lett.* **2023**, *8* (10), 4162−4172.

(14) Kuan, C.-H.; Afraj, S. N.; Huang, Y.-L.; Velusamy, A.; Liu, C.-L.; Su, T.-Y.; Jiang, X.; Lin, J.-M.; Chen, M.-C.; Diau, E. W.-G. Functionalized Thienopyrazines on NiOx Film as Self-Assembled Monolayer for Efficient Tin-Perovskite Solar Cells Using a Two-Step Method. *Angew. Chem., Int. Ed.* **2024**, *63* (39), No. e202407228.

(15) Phung, N.; Verheijen, M.; Todinova, A.; Datta, K.; Verhage, M.; Al-Ashouri, A.; Köbler, H.; Li, X.; Abate, A.; Albrecht, S.; Creatore, M. Enhanced Self-Assembled Monolayer Surface Coverage by ALD NiO in p-i-n Perovskite Solar Cells. *ACS Appl. Mater. Interfaces* **2022**, *14* (1), 2166−2176.

(16) Song, D.; Narra, S.; Li, M.-Y.; Lin, J.-S.; Diau, E. W.-G. Interfacial Engineering with a Hole-Selective Self-Assembled Monolayer for Tin Perovskite Solar Cells via a Two-Step Fabrication. *ACS Energy Lett.* **2021**, *6* (12), 4179−4186.

(17) Afraj, S. N.; Kuan, C.-H.; Lin, J.-S.; Ni, J.-S.; Velusamy, A.; Chen, M.-C.; Diau, E. W.-G. Quinoxaline-Based X-Shaped Sensitizers as Self-Assembled Monolayer for Tin Perovskite Solar Cells. *Adv. Funct. Mater.* **2023**, *33* (17), 2213939.

(18) Aktas, E.; Poli, I.; Ponti, C.; Li, G.; Olivati, A.; Di Girolamo, D.; Alharthi, F. A.; Li, M.; Palomares, E.; Petrozza, A.; Abate, A. One-Step Solution Deposition of Tin-Perovskite onto a Self-Assembled Monolayer with a DMSO-Free Solvent System. *ACS Energy Lett.* **2023**, *8* (12), 5170−5174.

(19) Cao, K.; Ning, H.; Xu, N.; Zuo, W.; Zhang, Y.; Yang, M.; Xia, J.; Liu, L.; Chen, S. Tailoring the Buried Interface with Self-Assembled 2-Chloroethylphosphonic Acid for Defect Reduction and Improved Performance of Tin-Based Perovskite Solar Cells. *J. Mater. Chem. A* **2024**, *12* (28), 17444−17452.

(20) Li, B.; Zhang, C.; Gao, D.; Sun, X.; Zhang, S.; Li, Z.; Gong, J.; Li, S.; Zhu, Z. Suppressing Oxidation at Perovskite-NiO Interface for Efficient and Stable Tin Perovskite Solar Cells. *Adv. Mater.* **2024**, *36* (17), 2309768.

(21) Abid, A.; Rajamanickam, P.; Wei-Guang Diau, E. Design of a Simple Bifunctional System as a Self-Assembled Monolayer (SAM) for Inverted Tin-Based Perovskite Solar Cells. *Chem. Eng. J.* **2023**, *477*, 146755.

(22) Al-Ashouri, A.; Köhnen, E.; Li, B.; Magomedov, A.; Hempel, H.; Caprioglio, P.; Márquez, J. A.; Morales Vilches, A. B.; Kasparavicius, E.; Smith, J. A.; Phung, N.; Menzel, D.; Grischek, M.; Kegelmann, L.; Skroblin, D.; Gollwitzer, C.; Malinauskas, T.; Jošt, M.; Matič, G.; Rech, B.; Schlatmann, R.; Topič, M.; Korte, L.; Abate, A.; Stannowski, B.; Neher, D.; Stolterfoht, M.; Unold, T.; Getautis, V.; Albrecht, S. Monolithic Perovskite/Silicon Tandem Solar Cell with > 29% Efficiency by Enhanced Hole Extraction. *Science* **2020**, *370* (6522), 1300−1309.

(23) Al-Ashouri, A.; Magomedov, A.; Roß, M.; Jošt, M.; Talaikis, M.; Chistiakova, G.; Bertram, T.; Márquez, J. A.; Köhnen, E.; Kasparavičius, E.; Levcenco, S.; Gil-Escrig, L.; Hages, C. J.; Schlatmann, R.; Rech, B.; Malinauskas, T.; Unold, T.; Kaufmann, C. A.; Korte, L.; Niaura, G.; Getautis, V.; Albrecht, S. Conformal Monolayer Contacts with Lossless Interfaces for Perovskite Single Junction and Monolithic Tandem Solar Cells. *Energy Environ. Sci.* **2019**, *12* (11), 3356−3369.

(24) Zheng, Y.; Li, Y.; Zhuang, R.; Wu, X.; Tian, C.; Sun, A.; Chen, C.; Guo, Y.; Hua, Y.; Meng, K.; Wu, K.; Chen, C.-C. Towards 26% Efficiency in Inverted Perovskite Solar Cells via Interfacial Flipped

https://doi.org/10.1021/acsenergylett.4c03228
ACS Energy Lett. 2025, 10, 1292−1312

Band Bending and Suppressed Deep-Level Traps. *Energy Environ. Sci.* **2024**, *17* (3), 1153−1162.
(25) Chen, J.; Luo, J.; Hou, E.; Song, P.; Li, Y.; Sun, C.; Feng, W.; Cheng, S.; Zhang, H.; Xie, L.; Tian, C.; Wei, Z. Efficient Tin-Based Perovskite Solar Cells with Trans-Isomeric Fulleropyrrolidine Additives. *Nat. Photonics* **2024**, *18* (5), 464−470.
(26) Magomedov, A.; Al-Ashouri, A.; Kasparavičius, E.; Strazdaite, S.; Niaura, G.; Jošt, M.; Malinauskas, T.; Albrecht, S.; Getautis, V. Self-Assembled Hole Transporting Monolayer for Highly Efficient Perovskite Solar Cells. *Adv. Energy Mater.* **2018**, *8* (32), 1801892.
(27) *NREL, Best Research-Cell Efficiency Chart*, https://www.nrel.gov/pv/assets/pdfs/best-research-cell-efficiencies.pdf (Last accessed: July 22, 2024).
(28) Ren, Z.; Cui, Z.; Shi, X.; Wang, L.; Dou, Y.; Wang, F.; Lin, H.; Yan, H.; Chen, S. Poly(Carbazole Phosphonic Acid) as a Versatile Hole-Transporting Material for p-i-n Perovskite Solar Cells and Modules. *Joule* **2023**, *7* (12), 2894−2904.
(29) Han, P.; Zhang, Y. Recent Advances in Carbazole-Based Self-Assembled Monolayer for Solution-Processed Optoelectronic Devices. *Adv. Mater.* **2024**, *36* (33), 2405630.
(30) Guo, R.; Wang, X.; Jia, X.; Guo, X.; Li, J.; Li, Z.; Sun, K.; Jiang, X.; Alvianto, E.; Shi, Z.; Schwartzkopf, M.; Müller-Buschbaum, P.; Hou, Y. Refining the Substrate Surface Morphology for Achieving Efficient Inverted Perovskite Solar Cells. *Adv. Energy Mater.* **2023**, *13* (43), 2302280.
(31) Wu, M.; Li, X.; Ying, Z.; Chen, Y.; Wang, X.; Zhang, M.; Su, S.; Guo, X.; Sun, J.; Shou, C.; Yang, X.; Ye, J. Reconstruction of the Indium Tin Oxide Surface Enhances the Adsorption of High-Density Self-Assembled Monolayer for Perovskite/Silicon Tandem Solar Cells. *Adv. Funct. Mater.* **2023**, *33* (46), 2304708.
(32) Tang, H.; Shen, Z.; Shen, Y.; Yan, G.; Wang, Y.; Han, Q.; Han, L. Reinforcing Self-Assembly of Hole Transport Molecules for Stable Inverted Perovskite Solar Cells. *Science* **2024**, *383* (6688), 1236−1240.
(33) Zhang, S.; Ye, F.; Wang, X.; Chen, R.; Zhang, H.; Zhan, L.; Jiang, X.; Li, Y.; Ji, X.; Liu, S.; Yu, M.; Yu, F.; Zhang, Y.; Wu, R.; Liu, Z.; Ning, Z.; Neher, D.; Han, L.; Lin, Y.; Tian, H.; Chen, W.; Stolterfoht, M.; Zhang, L.; Zhu, W.-H.; Wu, Y. Minimizing Buried Interfacial Defects for Efficient Inverted Perovskite Solar Cells. *Science* **2023**, *380* (6643), 404−409.
(34) Liu, M.; Bi, L.; Jiang, W.; Zeng, Z.; Tsang, S.-W.; Lin, F. R.; Jen, A. K.-Y. Compact Hole-Selective Self-Assembled Monolayers Enabled by Disassembling Micelles in Solution for Efficient Perovskite Solar Cells. *Adv. Mater.* **2023**, *35* (46), 2304415.
(35) Perera, W. H. K.; Masteghin, M. G.; Shim, H.; Davies, J. D.; Ryan, J. L.; Hinder, S. J.; Yun, J. S.; Zhang, W.; Jayawardena, K. D. G. I.; Silva, S. R. P. Modification of Hydrophobic Self-Assembled Monolayers with Nanoparticles for Improved Wettability and Enhanced Carrier Lifetimes Over Large Areas in Perovskite Solar Cells. *Solar RRL* **2023**, *7* (17), 2300388.
(36) Li, G.; Su, Z.; Canil, L.; Hughes, D.; Aldamasy, M. H.; Dagar, J.; Trofimov, S.; Wang, L.; Zuo, W.; Jerónimo-Rendon, J. J.; Byranvand, M. M.; Wang, C.; Zhu, R.; Zhang, Z.; Yang, F.; Nasti, G.; Naydenov, B.; Tsoi, W. C.; Li, Z.; Gao, X.; Wang, Z.; Jia, Y.; Unger, E.; Saliba, M.; Li, M.; Abate, A. Highly Efficient P-i-n Perovskite Solar Cells That Endure Temperature Variations. *Science* **2023**, *379* (6630), 399−403.
(37) Wang, Y.; Liao, Q.; Chen, J.; Huang, W.; Zhuang, X.; Tang, Y.; Li, B.; Yao, X.; Feng, X.; Zhang, X.; Su, M.; He, Z.; Marks, T. J.; Facchetti, A.; Guo, X. Teaching an Old Anchoring Group New Tricks: Enabling Low-Cost, Eco-Friendly Hole-Transporting Materials for Efficient and Stable Perovskite Solar Cells. *J. Am. Chem. Soc.* **2020**, *142* (39), 16632−16643.
(38) Zhang, Z.; Zhu, R.; Tang, Y.; Su, Z.; Hu, S.; Zhang, X.; Zhang, J.; Zhao, J.; Xue, Y.; Gao, X.; Li, G.; Pascual, J.; Abate, A.; Li, M. Anchoring Charge Selective Self-Assembled Monolayers for Tin-Lead Perovskite Solar Cells. *Adv. Mater.* **2024**, *36* (18), 2312264.
(39) Guo, H.; Liu, C.; Hu, H.; Zhang, S.; Ji, X.; Cao, X.-M.; Ning, Z.; Zhu, W.-H.; Tian, H.; Wu, Y. Neglected Acidity Pitfall: Boric Acid-Anchoring Hole-Selective Contact for Perovskite Solar Cells. *Natl. Sci. Rev.* **2023**, *10* (5), nwad057.
(40) Wu, J.; Yan, P.; Yang, D.; Guan, H.; Yang, S.; Cao, X.; Liao, X.; Ding, P.; Sun, H.; Ge, Z. Bisphosphonate-Anchored Self-Assembled Molecules with Larger Dipole Moments for Efficient Inverted Perovskite Solar Cells with Excellent Stability. *Adv. Mater.* **2024**, *36* (28), 2401537.
(41) Truong, M. A.; Funasaki, T.; Ueberricke, L.; Nojo, W.; Murdey, R.; Yamada, T.; Hu, S.; Akatsuka, A.; Sekiguchi, N.; Hira, S.; Xie, L.; Nakamura, T.; Shioya, N.; Kan, D.; Tsuji, Y.; Iikubo, S.; Yoshida, H.; Shimakawa, Y.; Hasegawa, T.; Kanemitsu, Y.; Suzuki, T.; Wakamiya, A. Tripodal Triazatruxene Derivative as a Face-On Oriented Hole-Collecting Monolayer for Efficient and Stable Inverted Perovskite Solar Cells. *J. Am. Chem. Soc.* **2023**, *145* (13), 7528−7539.
(42) Li, C.; Zhang, Z.; Zhang, H.; Yan, W.; Li, Y.; Liang, L.; Yu, W.; Yu, X.; Wang, Y.; Yang, Y.; Nazeeruddin, M. K.; Gao, P. Fully Aromatic Self-Assembled Hole-Selective Layer toward Efficient Inverted Wide-Bandgap Perovskite Solar Cells with Ultraviolet Resistance. *Angew. Chem., Int. Ed.* **2024**, *63* (1), No. e202315281.
(43) Aktas, E.; Phung, N.; Köbler, H.; González, D. A.; Méndez, M.; Kafedjiska, I.; Turren-Cruz, S.-H.; Wenisch, R.; Lauermann, I.; Abate, A.; Palomares, E. Understanding the Perovskite/Self-Assembled Selective Contact Interface for Ultra-Stable and Highly Efficient p-i-n Perovskite Solar Cells. *Energy Environ. Sci.* **2021**, *14* (7), 3976−3985.
(44) Dai, Z.; You, S.; Chakraborty, D.; Li, S.; Zhang, Y.; Ranka, A.; Barlow, S.; Berry, J. J.; Marder, S. R.; Guo, P.; Qi, Y.; Zhu, K.; Padture, N. P. Connecting Interfacial Mechanical Adhesion, Efficiency, and Operational Stability in High Performance Inverted Perovskite Solar Cells. *ACS Energy Lett.* **2024**, *9* (4), 1880−1887.
(45) Sun, A.; Tian, C.; Zhuang, R.; Chen, C.; Zheng, Y.; Wu, X.; Tang, C.; Liu, Y.; Li, Z.; Ouyang, B.; Du, J.; Li, Z.; Cai, J.; Chen, J.; Wu, X.; Hua, Y.; Chen, C.-C. High Open-Circuit Voltage (1.197 V) in Large-Area (1 Cm2) Inverted Perovskite Solar Cell via Interface Planarization and Highly Polar Self-Assembled Monolayer. *Adv. Energy Mater.* **2024**, *14* (8), 2303941.
(46) Jiang, W.; Li, F.; Li, M.; Qi, F.; Lin, F. R.; Jen, A. K.-Y. π-Expanded Carbazoles as Hole-Selective Self-Assembled Monolayers for High-Performance Perovskite Solar Cells. *Angew. Chem., Int. Ed.* **2022**, *61* (51), No. e202213560.
(47) Jiang, W.; Hu, Y.; Li, F.; Lin, F. R.; Jen, A. K.-Y. Hole-Selective Contact with Molecularly Tailorable Reactivity for Passivating High-Performing Inverted Perovskite Solar Cells. *CCS Chemistry* **2024**, *6* (7), 1654−1661.
(48) Hung, C.-M.; Mai, C.-L.; Wu, C.-C.; Chen, B.-H.; Lu, C.-H.; Chu, C.-C.; Wang, M.-C.; Yang, S.-D.; Chen, H.-C.; Yeh, C.-Y.; Chou, P.-T. Self-Assembled Monolayers of Bi-Functionalized Porphyrins: A Novel Class of Hole-Layer-Coordinating Perovskites and Indium Tin Oxide in Inverted Solar Cells. *Angew. Chem., Int. Ed.* **2023**, *62* (40), No. e202309831.
(49) Wang, Q.; Chueh, C.-C.; Zhao, T.; Cheng, J.; Eslamian, M.; Choy, W. C. H.; Jen, A. K.-Y. Effects of Self-Assembled Monolayer Modification of Nickel Oxide Nanoparticles Layer on the Performance and Application of Inverted Perovskite Solar Cells. *ChemSusChem* **2017**, *10* (19), 3794−3803.
(50) Liu, L.; Yang, Y.; Du, M.; Cao, Y.; Ren, X.; Zhang, L.; Wang, H.; Zhao, S.; Wang, K.; Liu, S. (Frank). Self-Assembled Amphiphilic Monolayer for Efficient and Stable Wide-Bandgap Perovskite Solar Cells. *Adv. Energy Mater.* **2023**, *13* (4), 2202802.
(51) Liu, M.; Li, M.; Li, Y.; An, Y.; Yao, Z.; Fan, B.; Qi, F.; Liu, K.; Yip, H.-L.; Lin, F. R.; Jen, A. K.-Y. Defect-Passivating and Stable Benzothiophene-Based Self-Assembled Monolayer for High-Performance Inverted Perovskite Solar Cells. *Adv. Energy Mater.* **2024**, *14* (12), 2303742.
(52) Ullah, A.; Park, K. H.; Lee, Y.; Park, S.; Faheem, A. B.; Nguyen, H. D.; Siddique, Y.; Lee, K.K.; Jo, Y.; Han, C.H.; Ahn, S.; Jeong, I.; Cho, S.; Kim, B.; Park, Y. S.; Hong, S. Versatile Hole Selective Molecules Containing a Series of Heteroatoms as Self-Assembled

https://doi.org/10.1021/acsenergylett.4c03228
ACS Energy Lett. 2025, 10, 1292−1312

Monolayers for Efficient p-i-n Perovskite and Organic Solar Cells. *Adv. Funct. Mater.* **2022**, *32* (49), 2208793.
(53) Al-Ashouri, A.; Marčinskas, M.; Kasparavičius, E.; Malinauskas, T.; Palmstrom, A.; Getautis, V.; Albrecht, S.; McGehee, M. D.; Magomedov, A. Wettability Improvement of a Carbazole-Based Hole-Selective Monolayer for Reproducible Perovskite Solar Cells. *ACS Energy Lett.* **2023**, *8* (2), 898−900.
(54) Deng, X.; Qi, F.; Li, F.; Wu, S.; Lin, F. R.; Zhang, Z.; Guan, Z.; Yang, Z.; Lee, C.-S.; Jen, A. K.-Y. Co-Assembled Monolayers as Hole-Selective Contact for High-Performance Inverted Perovskite Solar Cells with Optimized Recombination Loss and Long-Term Stability. *Angew. Chem., Int. Ed.* **2022**, *61* (30), No. e202203088.
(55) Li, L.; Wang, Y.; Wang, X.; Lin, R.; Luo, X.; Liu, Z.; Zhou, K.; Xiong, S.; Bao, Q.; Chen, G.; Tian, Y.; Deng, Y.; Xiao, K.; Wu, J.; Saidaminov, M. I.; Lin, H.; Ma, C.-Q.; Zhao, Z.; Wu, Y.; Zhang, L.; Tan, H. Flexible All-Perovskite Tandem Solar Cells Approaching 25% Efficiency with Molecule-Bridged Hole-Selective Contact. *Nat. Energy* **2022**, *7* (8), 708−717.
(56) Hossain, K.; Kulkarni, A.; Bothra, U.; Klingebiel, B.; Kirchartz, T.; Saliba, M.; Kabra, D. Resolving the Hydrophobicity of the Me-4PACz Hole Transport Layer for Inverted Perovskite Solar Cells with Efficiency > 20%. *ACS Energy Lett.* **2023**, *8* (9), 3860−3867.
(57) Ren, Z.; Cui, Z.; Shi, X.; Wang, L.; Dou, Y.; Wang, F.; Lin, H.; Yan, H.; Chen, S. Poly(Carbazole Phosphonic Acid) as a Versatile Hole-Transporting Material for p-i-n Perovskite Solar Cells and Modules. *Joule* **2023**, *7* (12), 2894−2904.
(58) Chang, C.-Y.; Huang, H.-H.; Tsai, H.; Lin, S.-L.; Liu, P.-H.; Chen, W.; Hsu, F.-C.; Nie, W.; Chen, Y.-F.; Wang, L. Facile Fabrication of Self-Assembly Functionalized Polythiophene Hole Transporting Layer for High Performance Perovskite Solar Cells. *Adv. Sci.* **2021**, *8* (5), 2002718.
(59) Paniagua, S. A.; Giordano, A. J.; Smith, O. L.; Barlow, S.; Li, H.; Armstrong, N. R.; Pemberton, J. E.; Brédas, J.-L.; Ginger, D.; Marder, S. R. Phosphonic Acids for Interfacial Engineering of Transparent Conductive Oxides. *Chem. Rev.* **2016**, *116* (12), 7117−7158.
(60) Li, C.; Chen, Y.; Zhang, Z.; Liu, C.; Guo, F.; Ahmad, W.; Gao, P. Pros and Cons of Hole-Selective Self-Assembled Monolayers in Inverted PSCs and TSCs: Extensive Case Studies and Data Analysis. *Energy Environ. Sci.* **2024**, *17* (17), 6157−6203.
(61) Hung, C.-M.; Wu, C.-C.; Yang, Y.-H.; Chen, B.-H.; Lu, C.-H.; Chu, C.-C.; Cheng, C.-H.; Yang, C.-Y.; Lin, Y.-D.; Cheng, C.-H.; Chen, J.-Y.; Ni, I.-C.; Wu, C.-I.; Yang, S.-D.; Chen, H.-C.; Chou, P.-T. Repairing Interfacial Defects in Self-Assembled Monolayers for High-Efficiency Perovskite Solar Cells and Organic Photovoltaics through the SAM@Pseudo-Planar Monolayer Strategy. *Adv. Sci.* **2024**, *11* (36), 2404725.
(62) Cassella, E. J.; Spooner, E. L. K.; Thornber, T.; O'Kane, M. E.; Catley, T. E.; Bishop, J. E.; Smith, J. A.; Game, O. S.; Lidzey, D. G. Gas-Assisted Spray Coating of Perovskite Solar Cells Incorporating Sprayed Self-Assembled Monolayers. *Adv. Sci.* **2022**, *9* (14), 2104848.
(63) Zheng, X.; Li, Z.; Zhang, Y.; Chen, M.; Liu, T.; Xiao, C.; Gao, D.; Patel, J. B.; Kuciauskas, D.; Magomedov, A.; Scheidt, R. A.; Wang, X.; Harvey, S. P.; Dai, Z.; Zhang, C.; Morales, D.; Pruett, H.; Wieliczka, B. M.; Kirmani, A. R.; Padture, N. P.; Graham, K. R.; Yan, Y.; Nazeeruddin, M. K.; McGehee, M. D.; Zhu, Z.; Luther, J. M. Co-Deposition of Hole-Selective Contact and Absorber for Improving the Processability of Perovskite Solar Cells. *Nat. Energy* **2023**, *8* (5), 462−472.
(64) Farag, A.; Feeney, T.; Hossain, I. M.; Schackmar, F.; Fassl, P.; Küster, K.; Bäuerle, R.; Ruiz-Preciado, M. A.; Hentschel, M.; Ritzer, D. B.; Diercks, A.; Li, Y.; Nejand, B. A.; Laufer, F.; Singh, R.; Starke, U.; Paetzold, U. W. Evaporated Self-Assembled Monolayer Hole Transport Layers: Lossless Interfaces in p-i-n Perovskite Solar Cells. *Adv. Energy Mater.* **2023**, *13* (8), 2203982.
(65) Yu, S.; Xiong, Z.; Zhou, H.; Zhang, Q.; Wang, Z.; Ma, F.; Qu, Z.; Zhao, Y.; Chu, X.; Zhang, X.; You, J. Homogenized NiOx Nanoparticles for Improved Hole Transport in Inverted Perovskite Solar Cells. *Science* **2023**, *382* (6677), 1399−1404.
(66) Wang, S.; Khan, D.; Zhou, W.; Sui, Y.; Zhang, T.; Yu, G.; Huang, Y.; Yang, X.; Chen, X.; Yan, H.; Tang, J.; Yang, F.; Han, P.; Zheng, Z.; Zhang, Y.; Tang, Z. Ion-Dipole Interaction for Self-Assembled Monolayers: A New Strategy for Buried Interface in Inverted Perovskite Solar Cells. *Adv. Funct. Mater.* **2024**, *34* (27), 2316202.
(67) Peng, W.; Mao, K.; Cai, F.; Meng, H.; Zhu, Z.; Li, T.; Yuan, S.; Xu, Z.; Feng, X.; Xu, J.; McGehee, M. D.; Xu, J. Reducing Nonradiative Recombination in Perovskite Solar Cells with a Porous Insulator Contact. *Science* **2023**, *379* (6633), 683−690.
(68) Kulkarni, A.; Sarkar, R.; Akel, S.; Häser, M.; Klingebiel, B.; Wuttig, M.; Wiegand, S.; Chakraborty, S.; Saliba, M.; Kirchartz, T. A Universal Strategy of Perovskite Ink - Substrate Interaction to Overcome the Poor Wettability of a Self-Assembled Monolayer for Reproducible Perovskite Solar Cells. *Adv. Funct. Mater.* **2023**, *33* (47), 2305812.
(69) Azmi, R.; Ugur, E.; Seitkhan, A.; Aljamaan, F.; Subbiah, A. S.; Liu, J.; Harrison, G. T.; Nugraha, M. I.; Eswaran, M. K.; Babics, M.; Chen, Y.; Xu, F.; Allen, T. G.; Rehman, A. ur; Wang, C.-L.; Anthopoulos, T. D.; Schwingenschlögl, U.; De Bastiani, M.; Aydin, E.; De Wolf, S. Damp Heat-Stable Perovskite Solar Cells with Tailored-Dimensionality 2D/3D Heterojunctions. *Science* **2022**, *376* (6588), 73−77.
(70) Song, D.; Li, H.; Xu, Y.; Yu, Q. Amplifying Hole Extraction Characteristics of PEDOT:PSS via Post-Treatment with Aromatic Diammonium Acetates for Tin Perovskite Solar Cells. *ACS Energy Lett.* **2023**, *8* (8), 3280−3287.
(71) Liu, J.; Li, S.; Mei, A.; Han, H. Applications of Metal Oxide Charge Transport Layers in Perovskite Solar Cells. *Small Sci.* **2023**, *3* (9), 2300020.
(72) Yin, M.; Yao, H.; Qiu, H.; Wu, C.; Zhang, M.; Hao, F. A Revisit of Crystallization in Tin Halide Perovskite Thin Films: From Nucleation, Intermediate to Crystal Growth. *Adv. Funct. Mater.* **2024**, *34* (39), 2404792.
(73) Dong, H.; Ran, C.; Gao, W.; Sun, N.; Liu, X.; Xia, Y.; Chen, Y.; Huang, W. Crystallization Dynamics of Sn-Based Perovskite Thin Films: Toward Efficient and Stable Photovoltaic Devices. *Adv. Energy Mater.* **2022**, *12* (1), 2102213.
(74) Zhu, Z.; Jiang, X.; Yu, D.; Yu, N.; Ning, Z.; Mi, Q. Smooth and Compact FASnI3 Films for Lead-Free Perovskite Solar Cells with over 14% Efficiency. *ACS Energy Lett.* **2022**, *7* (6), 2079−2083.
(75) Nasti, G.; Aldamasy, M. H.; Flatken, M. A.; Musto, P.; Matczak, P.; Dallmann, A.; Hoell, A.; Musiienko, A.; Hempel, H.; Aktas, E.; Di Girolamo, D.; Pascual, J.; Li, G.; Li, M.; Mercaldo, L. V.; Veneri, P. D.; Abate, A. Pyridine Controlled Tin Perovskite Crystallization. *ACS Energy Lett.* **2022**, *7* (10), 3197−3203.
(76) Jokar, E.; Chien, C.-H.; Fathi, A.; Rameez, M.; Chang, Y.-H.; Diau, E. W.-G. Slow Surface Passivation and Crystal Relaxation with Additives to Improve Device Performance and Durability for Tin-Based Perovskite Solar Cells. *Energy Environ. Sci.* **2018**, *11* (9), 2353−2362.
(77) Shao, S.; Liu, J.; Portale, G.; Fang, H.-H.; Blake, G. R.; ten Brink, G. H.; Koster, L. J. A.; Loi, M. A. Highly Reproducible Sn-Based Hybrid Perovskite Solar Cells with 9% Efficiency. *Adv. Energy Mater.* **2018**, *8* (4), 1702019.
(78) Bi, C.; Wang, Q.; Shao, Y.; Yuan, Y.; Xiao, Z.; Huang, J. Non-Wetting Surface-Driven High-Aspect-Ratio Crystalline Grain Growth for Efficient Hybrid Perovskite Solar Cells. *Nat. Commun.* **2015**, *6* (1), 7747.
(79) Meng, X.; Lin, J.; Liu, X.; He, X.; Wang, Y.; Noda, T.; Wu, T.; Yang, X.; Han, L. Highly Stable and Efficient FASnI3-Based Perovskite Solar Cells by Introducing Hydrogen Bonding. *Adv. Mater.* **2019**, *31* (42), 1903721.
(80) Su, Y.; Yang, J.; Liu, G.; Sheng, W.; Zhang, J.; Zhong, Y.; Tan, L.; Chen, Y. Acetic Acid-Assisted Synergistic Modulation of Crystallization Kinetics and Inhibition of Sn2+ Oxidation in Tin-Based Perovskite Solar Cells. *Adv. Funct. Mater.* **2022**, *32* (12), 2109631.

https://doi.org/10.1021/acsenergylett.4c03228
ACS Energy Lett. 2025, 10, 1292−1312

(81) Cui, D.; Liu, X.; Wu, T.; Lin, X.; Luo, X.; Wu, Y.; Segawa, H.; Yang, X.; Zhang, Y.; Wang, Y.; Han, L. Making Room for Growing Oriented FASnI3 with Large Grains via Cold Precursor Solution. *Adv. Funct. Mater.* **2021**, *31* (25), 2100931.
(82) Liu, J.; Ozaki, M.; Yakumaru, S.; Handa, T.; Nishikubo, R.; Kanemitsu, Y.; Saeki, A.; Murata, Y.; Murdey, R.; Wakamiya, A. Lead-Free Solar Cells Based on Tin Halide Perovskite Films with High Coverage and Improved Aggregation. *Angew. Chem., Int. Ed.* **2018**, *57* (40), 13221−13225.
(83) Su, Y.; Yang, J.; Rao, H.; Zhong, Y.; Sheng, W.; Tan, L.; Chen, Y. Environmentally Friendly Anti-Solvent Engineering for High-Efficiency Tin-Based Perovskite Solar Cells. *Energy Environ. Sci.* **2023**, *16* (5), 2177−2186.
(84) Dong, J.; Shao, S.; Kahmann, S.; Rommens, A. J.; Hermida-Merino, D.; ten Brink, G. H.; Loi, M. A.; Portale, G. Mechanism of Crystal Formation in Ruddlesden-Popper Sn-Based Perovskites. *Adv. Funct. Mater.* **2020**, *30* (24), 2001294.
(85) Chen, S.; Dai, X.; Xu, S.; Jiao, H.; Zhao, L.; Huang, J. Stabilizing Perovskite-Substrate Interfaces for High-Performance Perovskite Modules. *Science* **2021**, *373* (6557), 902−907.
(86) Treglia, A.; Prato, M.; Wu, C.-S. J.; Wong, E. L.; Poli, I.; Petrozza, A. Understanding the Surface Chemistry of Tin Halide Perovskites. *Adv. Funct. Mater.* **2024**, *34* (42), 2406954.
(87) Jokar, E.; Cheng, P.-Y.; Lin, C.-Y.; Narra, S.; Shahbazi, S.; Wei-Guang Diau, E. Enhanced Performance and Stability of 3D/2D Tin Perovskite Solar Cells Fabricated with a Sequential Solution Deposition. *ACS Energy Lett.* **2021**, *6* (2), 485−492.
(88) Zhang, Z.; Kamarudin, M. A.; Baranwal, A. K.; Kapil, G.; Sahamir, S. R.; Sanehira, Y.; Chen, M.; Wang, L.; Shen, Q.; Hayase, S. Sequential Passivation for Lead-Free Tin Perovskite Solar Cells with High Efficiency. *Angew. Chem., Int. Ed.* **2022**, *61* (42), No. e202210101.
(89) Li, H.; Chang, B.; Wang, L.; Wang, Z.; Pan, L.; Wu, Y.; Liu, Z.; Yin, L. Surface Reconstruction for Tin-Based Perovskite Solar Cells. *ACS Energy Lett.* **2022**, *7* (11), 3889−3899.
(90) Jiang, X.; Wang, F.; Wei, Q.; Li, H.; Shang, Y.; Zhou, W.; Wang, C.; Cheng, P.; Chen, Q.; Chen, L.; Ning, Z. Ultra-High Open-Circuit Voltage of Tin Perovskite Solar Cells via an Electron Transporting Layer Design. *Nat. Commun.* **2020**, *11* (1), 1245.
(91) Sun, C.; Yang, P.; Nan, Z.; Tian, C.; Cai, Y.; Chen, J.; Qi, F.; Tian, H.; Xie, L.; Meng, L.; Wei, Z. Well-Defined Fullerene Bisadducts Enable High-Performance Tin-Based Perovskite Solar Cells. *Adv. Mater.* **2023**, *35* (9), 2205603.
(92) Kim, S. Y.; Cho, S. J.; Byeon, S. E.; He, X.; Yoon, H. J. Self-Assembled Monolayers as Interface Engineering Nanomaterials in Perovskite Solar Cells. *Adv. Energy Mater.* **2020**, *10* (44), 2002606.
(93) Chen, K.; Wu, P.; Yang, W.; Su, R.; Luo, D.; Yang, X.; Tu, Y.; Zhu, R.; Gong, Q. Low-Dimensional Perovskite Interlayer for Highly Efficient Lead-Free Formamidinium Tin Iodide Perovskite Solar Cells. *Nano Energy* **2018**, *49*, 411−418.
(94) Cao, J.-J.; Lou, Y.-H.; Yang, W.-F.; Wang, K.-L.; Su, Z.-H.; Chen, J.; Chen, C.-H.; Dong, C.; Gao, X.-Y.; Wang, Z.-K. Multifunctional Potassium Thiocyanate Interlayer for Eco-Friendly Tin Perovskite Indoor and Outdoor Photovoltaics. *Chem. Eng. J.* **2022**, *433*, 133832.
(95) Yu, B.-B.; Chen, Z.; Zhu, Y.; Wang, Y.; Han, B.; Chen, G.; Zhang, X.; Du, Z.; He, Z. Heterogeneous 2D/3D Tin-Halides Perovskite Solar Cells with Certified Conversion Efficiency Breaking 14%. *Adv. Mater.* **2021**, *33* (36), 2102055.
(96) Song, D.; Tseng, H.-Y.; Narra, S.; Tsai, I.-H.; Wei-Guang Diau, E. Solvent Engineering for Triple Cationic ITO-Based Mesoscopic Tin Perovskite Solar Cells. *Chem. Eng. J.* **2023**, *464*, 142635.
(97) Wu, T.; Liu, X.; Luo, X.; Lin, X.; Cui, D.; Wang, Y.; Segawa, H.; Zhang, Y.; Han, L. Lead-Free Tin Perovskite Solar Cells. *Joule* **2021**, *5* (4), 863−886.
(98) Singh, A.; Hieulle, J.; Machado, J. F.; Gharabeiki, S.; Zuo, W.; Farooq, M. U.; Phirke, H.; Saliba, M.; Redinger, A. Coevaporation Stabilizes Tin-Based Perovskites in a Single Sn-Oxidation State. *Nano Lett.* **2022**, *22* (17), 7112−7118.
(99) Meggiolaro, D.; Ricciarelli, D.; Alasmari, A. A.; Alasmary, F. A. S.; De Angelis, F. Tin versus Lead Redox Chemistry Modulates Charge Trapping and Self-Doping in Tin/Lead Iodide Perovskites. *J. Phys. Chem. Lett.* **2020**, *11* (9), 3546−3556.
(100) Liu, J.; Yao, H.; Wang, S.; Wu, C.; Ding, L.; Hao, F. Origins and Suppression of Sn(II)/Sn(IV) Oxidation in Tin Halide Perovskite Solar Cells. *Adv. Energy Mater.* **2023**, *13* (23), 2300696.
(101) Zhang, Z.; Huang, Y.; Jin, J.; Jiang, Y.; Xu, Y.; Zhu, J.; Zhao, D. Mechanistic Understanding of Oxidation of Tin-Based Perovskite Solar Cells and Mitigation Strategies. *Angew. Chem., Int. Ed.* **2023**, *62* (45), No. e202308093.
(102) Macdonald, T. J.; Lanzetta, L.; Liang, X.; Ding, D.; Haque, S. A. Engineering Stable Lead-Free Tin Halide Perovskite Solar Cells: Lessons from Materials Chemistry. *Adv. Mater.* **2023**, *35* (25), 2206684.
(103) Liu, H.; Zhang, Z.; Zuo, W.; Roy, R.; Li, M.; Byranvand, M. M.; Saliba, M. Pure Tin Halide Perovskite Solar Cells: Focusing on Preparation and Strategies. *Adv. Energy Mater.* **2023**, *13* (3), 2202209.
(104) Zhang, H.; Li, K.; Sun, M.; Wang, F.; Wang, H.; Jen, A. K.-Y. Design of Superhydrophobic Surfaces for Stable Perovskite Solar Cells with Reducing Lead Leakage. *Adv. Energy Mater.* **2021**, *11* (41), 2102281.
(105) de Boer, B.; Hadipour, A.; Mandoc, M. M.; van Woudenbergh, T.; Blom, P. W. M. Tuning of Metal Work Functions with Self-Assembled Monolayers. *Adv. Mater.* **2005**, *17* (5), 621−625.
(106) Polman, A.; Knight, M.; Garnett, E. C.; Ehrler, B.; Sinke, W. C. Photovoltaic Materials: Present Efficiencies and Future Challenges. *Science* **2016**, *352* (6283), aad4424.
(107) Zuraw, W.; Vinocour Pacheco, F. A.; Sánchez-Diaz, J.; Przypis, Ł.; Mejia Escobar, M. A.; Almosni, S.; Vescio, G.; Martínez-Pastor, J. P.; Garrido, B.; Kudrawiec, R.; Mora-Seró, I.; Öz, S. Large-Area, Flexible, Lead-Free Sn-Perovskite Solar Modules. *ACS Energy Lett.* **2023**, *8* (11), 4885−4887.

https://doi.org/10.1021/acsenergylett.4c03228
ACS Energy Lett. 2025, 10, 1292−1312